Science of the Total Environment 915 (2024) 169989

Contents lists available at ScienceDirect

Science of the Total Environment

journal homepage: www.elsevier.com/locate/scitotenv

Long-term analysis of microseism during extreme weather events: Medicanes and common storms in the Mediterranean Sea

Alfio Marco Borzì [a,*], Vittorio Minio [b], Raphael De Plaen [c], Thomas Lecocq [c], Flavio Cannavò [b], Giuseppe Ciraolo [d], Sebastiano D'Amico [e], Carlo Lo Re [f], Carmelo Monaco [a,b,g], Marco Picone [f], Giovanni Scardino [h], Giovanni Scicchitano [h], Andrea Cannata [a,b]

[a] Dipartimento di Scienze Biologiche, Geologiche ed Ambientali – Sezione di Scienze della Terra, Università degli Studi di Catania, 95127 Catania, Italy
[b] Istituto Nazionale di Geofisica e Vulcanologia – Osservatorio Etneo, 95125 Catania, Italy
[c] Seismology-Gravimetry, Royal Observatory of Belgium, 1180 Brussels, Belgium
[d] Dipartimento di Ingegneria, Università degli Studi di Palermo, Bd. 8, 90128 Palermo, Italy
[e] Department of Geosciences, University of Malta, MSD 2080, Msida, Malta
[f] Italian Institute for Environmental Protection and Research (ISPRA), 00144 Rome, Italy
[g] CRUST-Interuniversity Center for 3D Seismotectonics with Territorial Applications, 66100 Chieti Scalo, Italy
[h] Dipartimento di Scienze della Terra e Geoambientali, Università degli Studi di Bari Aldo Moro, 70125 Bari, Italy

HIGHLIGHTS

- Spatial and temporal development of Medicanes and common storms was tracked by microseism, integrated with hindcast data.
- Medicanes show a seismic signature of 0.18-0.35 Hz while common storms of 0.3-0.7 Hz.
- Common storms show stronger seismic strength than Medicanes, in both cases, it is linked to sea extent with SWH > 3 m
- Integration of seismic signature and strength of these events help us to seismically distinguish Medicanes from common storms.
- The new approach developed in this work could be useful to analyze old seismograms in search of unknown Medicanes.

GRAPHICAL ABSTRACT

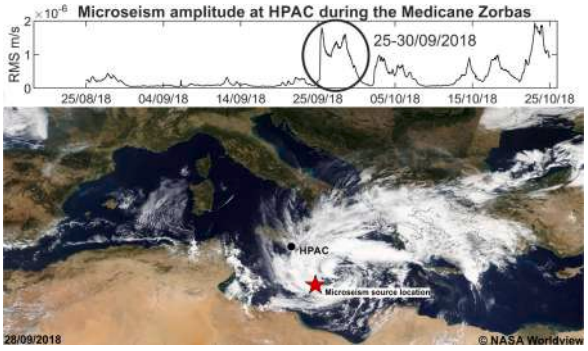

ARTICLE INFO

Editor: Christian Herrera

Keywords:
Microseism
Medicanes
Mediterranean Sea

ABSTRACT

In this work, we analyze 12 meteorological events that occurred in the Mediterranean Sea during the period November 2011–November 2021 from a seismic point of view. In particular, we consider 8 Medicanes and 4 more common storms. Each of these events, in spite of the marked differences between them, caused heavy rainfall, strong wind gusts and violent storm surge with significant wave heights usually >3 m. We deal with the relationships between these meteorological events and the features of microseism (the most continuous and widespread seismic signal on Earth) in terms of spectral content, space-time variation of the amplitude and

* Corresponding author at: Corso Italia 57, 95129 Catania, Italy.
E-mail address: alfio.borzi@phd.unict.it (A.M. Borzì).

https://doi.org/10.1016/j.scitotenv.2024.169989
Received 25 October 2023; Received in revised form 5 January 2024; Accepted 5 January 2024
Available online 14 January 2024

Common storms
Climate change
Monitoring sea state
Hindcast maps
Wave buoys

source locations tracked employing two different methods (amplitude decay-based grid search and array techniques). By comparing the positions of the microseism sources with the areas of significant storm surges, we observe that the microseism locations align with the actual locations of the storm surges for 10 out of 12 events analyzed (two Medicanes present very low intensity in terms of meteorological parameters and the microseism amplitude does not show significant variations during these two events). We also perform two analyses that allowed us to obtain both the seismic signature of these events, by using a method that exploits the coherence of continuous seismic noise, and their strength from a seismic point of view, called Microseism Reduced Amplitude. In addition, by integrating the results obtained from these two methods, we are able to "seismically" distinguish Medicanes and common storms. Consequently, we demonstrate the possibility of creating a novel monitoring system for Mediterranean meteorological events by incorporating microseism information alongside with other commonly employed techniques for studying meteorological phenomena. The integration of microseism with the data provided by routinely used techniques in sea state monitoring (e.g., wave buoy and HF radar) has the potential to offer valuable insights into the examination of historical extreme weather events within the context of climate change.

1. Introduction

In the last 12 years, several Medicanes (MEDIterranean hurriCANES) or TLC (Tropical Like Cyclones) took place in the Mediterranean Sea. These Mediterranean extreme weather events caused damages, floods, deaths and injuries in various places (South France, Central, and South Italy, Malta, Balearic islands, Greece, Crete, Turkey and some African states; Androulidakis et al., 2022; Bouin and Lebeaupin Brossier, 2020; Carrió et al., 2017; Dafis et al., 2018; Di Muzio et al., 2019; Faranda et al., 2022; Kerkmann and Bachmeier, 2011; Lagouvardos et al., 2022; Pravia-Sarabia et al., 2021; Portmann et al., 2020; Rumora et al., 2018; Varlas et al., 2020; Zimbo et al., 2022).

A Medicane is a small-scale tropical cyclone that develops over the Mediterranean Sea; these events have similar features to tropical cyclones, both in shape, observing them from satellite images, and in their dynamic and thermodynamic characteristics. Medicanes develop when an extratropical depression becomes isolated from the polar jet stream, resulting in a quasi-stationary "cut-off" feature above the Mediterranean Sea. This feature takes advantage of the abundant heat and humidity provided by the sea to generate organized convection (Faranda et al., 2022). The main characteristics of Medicanes include an "eye," a pronounced rotation around the low-pressure center, and an eyewall with convective cells that give rise to rain bands. These weather systems also bring about sea-level rise, storm surge, and significant sea waves, reaching heights of approximately five meters. Additionally, there is a warm-core anomaly that peaks near the surface (Miglietta and Rotunno, 2019). In contrast with tropical cyclones, due to the limited extent of the Mediterranean Sea that represents their major energy source, the Medicanes lifetime is restricted to a few days. Furthermore, their fully tropical characteristics are only attained for a brief period, with extratropical features prevailing for the majority of their lifespan (Miglietta et al., 2011, 2013). The average diameter of Medicanes is approximately 100–300 km (Comellas Prat et al., 2021), and their intensity rarely exceeds category 1 on the Saffir-Simpson hurricane wind scale (Miglietta and Rotunno, 2019). On average, we observe merely 1–2 events per year, typically occurring during the autumn months from September to January. In fact, the development of Medicane is favored during these five months when the Mediterranean Sea reaches its highest temperature following the summer season, coinciding with the arrival of the first cold jet stream (Cavicchia et al., 2014; Nastos et al., 2018). As explained by Cavicchia and von Storch (2012), the most frequent genesis regions are the Balearic Islands and the Ionian Sea. However, over the past 12 years, the majority of Medicanes have consistently formed over the Ionian Sea, which is likely attributed to the higher sea surface temperature in that area. Research by Shaltout and Omstedt (2014) has revealed that the Ionian Sea maintains a temperature that is consistently 1°-1.5 °C higher than the Tyrrhenian Sea.

Although these extreme Mediterranean events showed significant wave heights (hereinafter SWH; defined as the average wave height of the highest one-third of the waves) comparable to the common seasonal storms, they caused greater coastal flooding with respect to them because they can induce higher and longer surges along the coastline (Scicchitano et al., 2021; Scardino et al., 2022).

During the Medicanes lifetime, strong winds are generated. Since the Medicanes mostly stay offshore, the strong winds influence the sea state and cause the development of violent wave motions leading to an energy transfer from the sea waves to the solid Earth. This energy transfer generates the most continuous and ubiquitous seismic signal on the Earth, caused by the interaction between the atmosphere, the hydrosphere and the solid Earth, called microseism (e.g., Longuet-Higgins, 1950; Hasselmann, 1963). Considering the spectral content and the source mechanism (e.g., Haubrich and McCamy, 1969), it is possible to divide this signal into primary microseism (PM), secondary microseism (SM), and short-period secondary microseism (SPSM). The PM shows the same period of the oceanic waves (13–20 s) and the same spectral content; it is generated by the energy transfer of oceanic waves breaking against the shoreline and shows low amplitudes or by pressure fluctuations that propagate toward the sea floor near the coastal areas (Hasselmann, 1963; Ardhuin et al., 2015). The SM arises from sea waves propagating in opposite directions with identical frequencies and manifests with a frequency approximately twice that of the oceanic waves (with periods of 5–10 s). Additionally, the SM showcases higher amplitude compared to the PM (Longuet-Higgins, 1950; Oliver and Page, 1963; Ardhuin and Roland, 2012; Ardhuin et al., 2015). The SPSM has a period shorter than 5 s and is generated by the interaction between local wave motions near the coastline (Bromirski et al., 2005).

Several studies highlighted a correlation between microseism and the sea state (Ardhuin et al., 2019; Cannata et al., 2020; Moschella et al., 2020), and especially between microseism and cyclonic activity (e.g., Bromirski, 2001; Bromirski et al., 2005; Gerstoft et al., 2006; Gualtieri et al., 2018; Lin et al., 2017; Retailleau and Gualtieri, 2019, 2021; Zhang et al., 2010). Bromirski (2001) and Bromirski et al. (2005) showed the link between SM, SPSM, and cyclonic activity. Other authors treated the relationship between SM, SPSM, typhoons (Lin et al., 2017), tropical cyclones (Zhang et al., 2010), and hurricanes (Gerstoft et al., 2006). Specifically, Gerstoft et al. (2006) utilized the microseism recorded by a large-scale array to monitor the movement of Hurricane Katrina. Moreover, Retailleau and Gualtieri (2019) successfully tracked the trajectory of the 2006 typhoon Ioke by employing microseism, while Gualtieri et al. (2018) demonstrated a correlation between the spectral amplitude of microseism and the intensity of tropical cyclones. For the first time, the relationship between microseism and Medicane was analyzed by Borzì et al. (2022), who took into account the Medicane Apollo to analyze the power spectral density (hereinafter PSD) and root mean square (hereinafter RMS) amplitude time-variation and its seismic position during its lifetime by using two different methods (i.e. array analysis and grid search method based on seismic amplitude decay).

From Borzì et al. (2022) and Borzì et al. (2024), it is evident that it is possible to extract information about the Medicanes by using microseism data and in particular that the microseism bands which show a

higher correlation with Medicanes are the SM and SPSM. These first approaches are limited, however, only to track the variation of microseism amplitude during the Medicane and its position (Borzì et al., 2022) and to retrieve the seismic signature of the quasi-Medicane Helios (Borzì et al., 2024). Some questions still remain open:

i) Do all the Medicanes share a similar seismic signature?
ii) Is it possible to retrieve the seismic intensity of Medicanes and common storms and to which meteorological parameters are more correlated?
iii) Is it possible to seismically distinguish Medicanes from more common storms?

To answer these questions, in this work, we investigate microseism recorded during 8 Medicanes and 4 common storms, which occurred in the Mediterranean Sea between November 2011 and October 2021. Using sea state data (hindcast and wave buoy data) and seismic data, we perform several analyses. In particular, we carry out spectral analysis, to show the spatio-temporal microseism amplitude variation, and location analyses (grid search approach and array technique) to track Medicanes during their lifetime. In addition, since the scientific community is particularly interested in climate change and how this can interact with the occurrence rate and the intensity of Medicanes and common storms, we apply a method, developed by Soubestre et al. (2018), that, exploiting the coherence of seismic noise across the network, allow us to obtain information about the seismic signature of these events. In addition, we define the Microseism Reduced Amplitude to calculate the strength of both Medicanes and common storms from a seismic point of view. The integration of the results retrieved from the two aforementioned methods allows us to distinguish Medicanes from more common storms. Hence, by applying these methods on old digitized seismograms (e.g., Lecocq et al., 2020), it would be possible to extract microseism information about old storm or Medicanes. This could be useful for broaden the statistics about these events and their occurrence rate and intensity in the climate change scenario.

2. Medicanes description

In this section, we describe the main features, both in meteorological terms (rainfall, wind gust, minimum pressure value, dimension and lifetime, SWH) and in terms of damage, caused by the 8 Medicanes and 4 common storms taken into account. We started our analysis from Rolf, in November 2011, both because it is the first official Medicane and for the availability of seismic data, while we ended the analysis with Apollo, in November 2021, since this Medicane is one of the last that occurred in the Mediterranean Sea. An overview map of the tracks of all the considered Medicanes is shown in Fig. 1. All the meteorological parameters that have characterized the Medicanes are summarized in Table 1.

2.1. Medicane "Rolf": 6–9 November 2011

The Medicane Rolf occurred on 6–9 November 2011 and started from a surface low-pressure system near the Balearic Islands (Supplementary Fig. 1) early on 6 November. Later on that day, the convective activity started, and on 7 November, the system exhibited tropical attributes such as a warm core and well-organized convective bands encircling a quasi-symmetric structure. On 8 November, Rolf reached its maximum intensity (991 hPa of central pressure and maximum 1-min sustained winds of 83 km/h), and the NOAA officially declared the system a tropical storm (NOAA, n.d). The same day, the Alghero buoy recorded SWH higher than 5 m with a period of between 6 and 8 s around the storm peak (Fig. 2a and d). On 9 November, however, the storm made landfall in south-eastern France, near Hyères (Supplementary Fig. 1), where strong wind gusts and rainfall were recorded and dissipated completely shortly thereafter (Kerkmann and Bachmeier, 2011). Rolf was the first tropical-like cyclone ever to be officially monitored by the NOAA in the Mediterranean Sea (Enrique Pravia-Sarabia et al., 2021). The Medicane "ROLF" was the longest-lasting and probably the most intense case of Medicane until 2011 (Dafis et al., 2018).

2.2. Medicane "Qendresa": 7–8 November 2014

From the first hours of 7 November, a small depression near Pantelleria (Supplementary Fig. 1) began to deepen. Although the center of the cyclone progressed eastwards some 100 km north of Lampedusa (Supplementary Fig. 1), the surface pressure records on the island showed a 10 hPa drop in 1.5 h and at the same time, the barometer installed in Malta island (Supplementary Fig. 1) recorded a pressure drop of nearly 20 hPa in 6 h, and a minimum recorded pressure for the event of 985 hPa on 7 November at 16:45 UTC. The wind record in Malta provided a clear signature of the structure of the eye, with intense wind speeds (gusts exceeding 153 km/h) that preceded and followed a relatively calm period. Ten hours later, the signature over the Catania (Supplementary Fig. 1) pressure record was much attenuated, with winds still showing a calm period followed by gusts reaching 140 km/h (Carrió et al., 2017). In addition, strong convection developed on the morning of 7 November with heavy precipitation (>150 mm locally) and damage, caused by the strong wind and rain observed in the islands of Pantelleria, Lampedusa (Supplementary Fig. 1), and Malta (Bouin and Lebeaupin Brossier, 2020). Finally, the small cyclonic system dissipated as it crossed the eastern coast of Sicily (Catania area) moving over land.

Measurements performed by the wave buoy of Crotone (Supplementary Fig. 1) and Catania (Fig. 2b) during the passage of Qendresa showed values of SWH of about 4 m with a period of about 6 s (Fig. 2e, Scicchitano et al., 2021).

2.3. Medicane "Xandra": 1–3 December 2014

From the first hours of 1 December 2014, a low-pressure system was observed in the west of Sardinia (Supplementary Fig. 1). In the following hours, the vortex, thanks to the high temperature of the Mediterranean Sea, acquired energy and on 2 December made landfall on the west coast of Sardinia. Despite being on land, it continued to intensify and moved westward, finding the sea again after a few hours. On 3 December, shortly before making landfall on the Latium coast, it acquired the characteristics of a Medicane and formed the cyclone eye. In the Ciociaria area (territory between Latium and Campania, Supplementary Fig. 1), strong wind gusts (up to 93 km/h), heavy rainfall (100 mm/24 h), flooding, and two deaths were recorded. The minimum pressure value was 989 hPa (Di Muzio et al., 2019), and the diameter of the vortex reached about 200 km. The Cagliari buoy recorded SWH of about 3 m for a short time interval during the night between 2 and 3 December (Fig. 2c and f).

2.4. Medicane "Trixie": 28 October-1 November 2016

During 27 October 2016, a tropical depression crossed over the Italian Peninsula, and on 28 October, after reaching the still-warm Ionian Sea, it acquired sub-tropical features. During the days 28–29 October, the vortex became more intense, and heavy rain (280 mm/24 h) and severe wind gusts were recorded in the Ragusa area (Supplementary Fig. 1). Subsequently, the vortex started its eastward shifts, and shortly before making landfall on the Greek coast, it became a Medicane. At Kythira (Supplementary Fig. 1), a wind gust of 120 km/h and rainfall of 102 mm/8 h were recorded. During the night between 31 October and 1 November, the Medicane lost energy and dissipated. From a barometric point of view, the Medicane Trixie was one of the weakest ever recorded (1002 hPa) but was very long-lived (about 5 days), and the diameter was 300 km (Di Muzio et al., 2019).

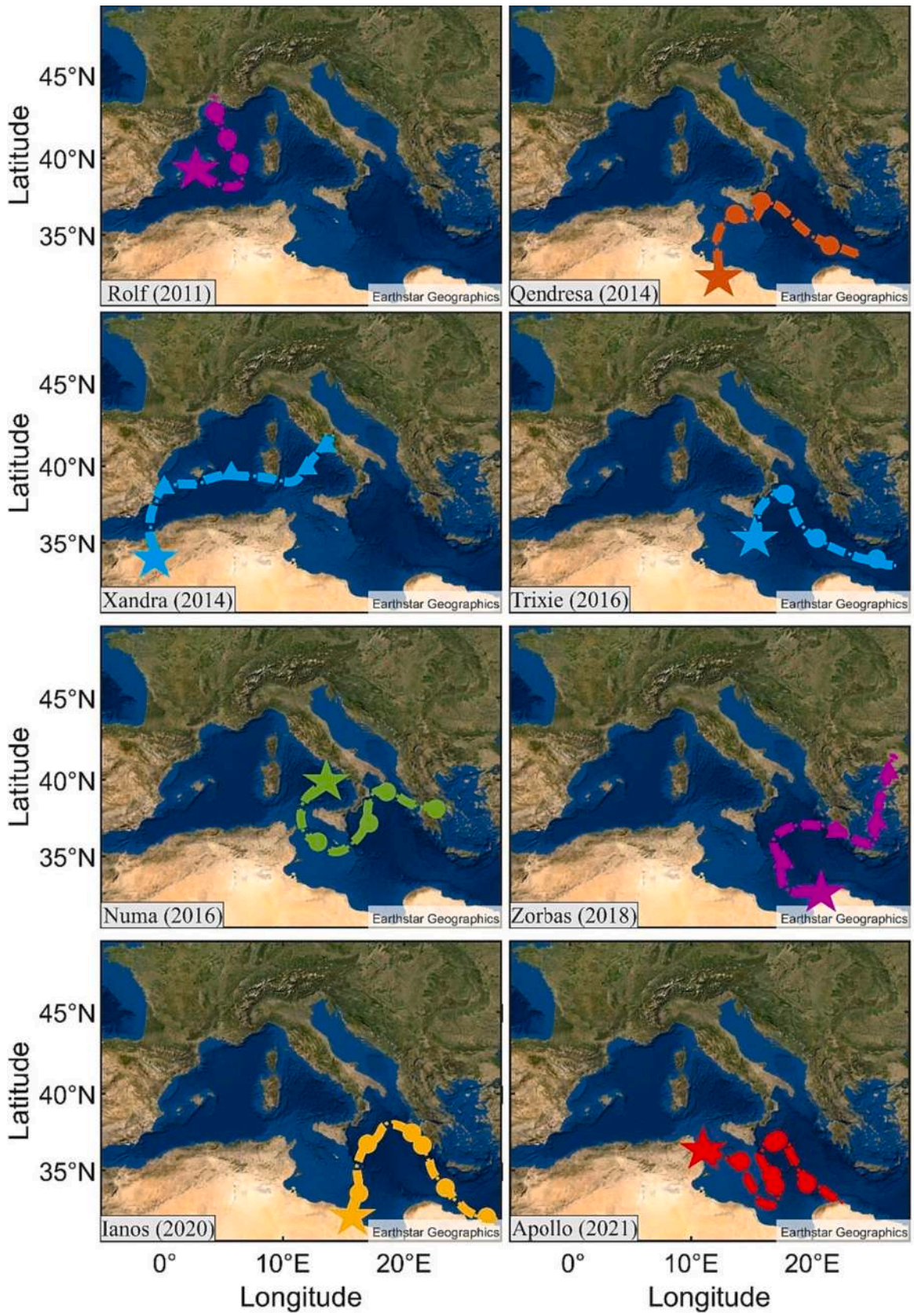

Fig. 1. Satellite image of the Mediterranean area with the track of the considered Medicanes. The stars indicate the starting position of the Medicanes. All the data regarding the position of the Medicanes were derived from the literature (Bouin and Brossier, 2020; Carrìo et al., 2017; Dafis et al., 2018; Di Muzio et al., 2019; Faranda et al., 2022; Lagouvardos et al., 2022; Portmann et al., 2020; Varlas et al., 2023). (base image source ©Earthstar Geographic).

Table 1
Main meteorological features of the 8 analyzed Medicanes. All these meteorological parameters were derived from the literature (Bouin and Brossier, 2020; Carrìo et al., 2017; Dafis et al., 2018; Di Muzio et al., 2019; Faranda et al., 2022; Lagouvardos et al., 2022; Portmann et al., 2020; Varlas et al., 2023).

Name	Rolf	Qendresa	Xandra	Trixie	Numa	Zorbas	Ianos	Apollo
Rain (mm/24 h)	\	>150	>100	280	\	100	200	>200
Max Wind Gust (km/h)	83	153	93	120	72	72	112	104
SWH (m)	>4	>4	1.5–2	>3.5	>3	>5	>5	>4
Minimum Pressure (hPa)	991	985	993	1002	1003	990	984	999
Duration (days)	4	2	3	5	5	4	5	4
Area with SWH > 3 m (km^2)	1.83E+05	6.25E+05	\	3.03E+05	\	4.56E+05	1.34E+05	1.61E+05
MRA (m^2/s)	0.1111	0.1270	\	0.0465	\	0.0680	0.0359	0.0403

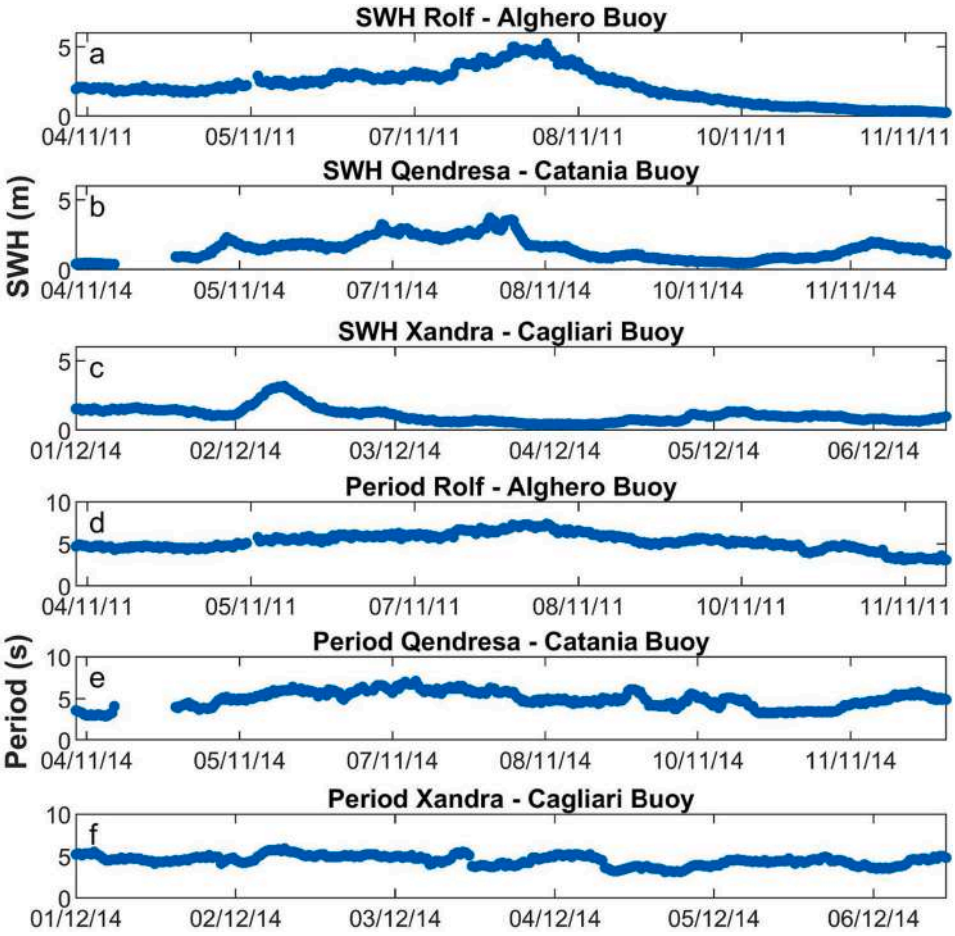

Fig. 2. Wave features in terms of SWH and period time series retrieved by using the Alghero (a and d), Catania (b and e) and Cagliari (c and f) buoy data. For the instruments location see Fig. 3a.

2.5. Medicane "Numa": 15–19 November 2017

Numa started as a low-pressure system over the Tyrrhenian area on 13–14 November on the remnants of an Atlantic Ocean anomaly that entered the Mediterranean Sea. The vortex became deeper while it was located south of Malta on 15 November. On the next day, it moved toward the east and, intensifying, acquired sub-tropical features. On 17 November, it became a Medicane and showed the typical Medicane characteristics (quasi-cloud-free eye, a warm core, and strong winds close to the vortex center). Then, it moved eastward, and, on 19 November, it completely dissipated over Greece. This Medicane caused loss of lives and substantial damage, first in central Mediterranean islands (Sicily, Malta, and other nearby minor islands) and southern Italy, and then in Greece (Rumora et al., 2018). The main features of the Medicane were a diameter of 230 km, a minimum pressure value of about 1003 hPa, a maximum wind gust recorded of 72 km/h near the cyclone eye, and heavy rainfall over southern Apulia.

2.6. Medicane "Zorbas": 27–30 September 2018

On 27 September 2018, a low-pressure system formed over the Gulf of Sidra (Supplementary Fig. 1) in the central-southern Mediterranean Sea. Successively, it moved over the southern Ionian Sea and southern Greece (28–29 September) and acquired Medicane features. It was possible to observe the formation of the cyclone eye just before making landfall on the Greek coast. Zorbas dissipated on 30 September. The Medicane affected an area of >400 km in radius, causing sustained winds that exceeded 72 km/h and resulting in high waves (> 5 m), and storm surges that caused inundation at coastal southwestern Greece (Varlas et al., 2020). The central pressure was estimated to reach approximately 990 hPa and was followed by intense rainfall, which exceeded 100 mm at some Greek areas, causing floods and extensive

damage to buildings, infrastructures, and agriculture (Portmann et al., 2020). This Medicane is considered one of the most energetic ever recorded and reached its maximum intensity only 12 h after cyclogenesis.

Evidence of this Medicane was observed along the rocky coast of the Maddalena Peninsula (Siracusa, Supplementary Fig. 1), where a surveillance camera of the Marine Protected Area of Plemmirio recorded several boulder displacements that occurred inside an ancient Greek quarry (Scicchitano et al., 2020).

2.7. Medicane "Ianos": 15–20 September 2020

The Medicane "Ianos" affected the Mediterranean basin from 15 to 20 September 2020. This Medicane caused extreme events (heavy rains, strong wind gusts, and storm surges) in southern Calabria, eastern Sicily, and in Greece. Ianos was generated from an Atlantic front isolated over the Mediterranean Sea, causing a low-pressure system in front of the coast of Tripoli on 14 September. In the following days, moving northwards and due to the high temperature of the sea (about 28 °C, 1.5 °C warmer than average), the vortex became more intense, and on 17 September, it acquired the typical Medicane characteristics with a minimum pressure value of 984 hPa (or slightly lower), a symmetrical structure with the formation of an eye, and a deep warm core. On the same day, the Medicane approached the Italian coast with heavy rainfall (123 mm/2 h) and severe wind gusts (90 km/h) that affected the Calabria region. Successively, the vortex started to move eastward, preserving its intensity until it made landfall on the Greek coast, where it caused intense wind gusts (112 km/h at Kefalonia airport, Supplementary Fig. 1), heavy rainfall with a pluviometric mean >200 mm/24 h, and >1400 landslides. Further damage was caused by the wave motions. Indeed, both in the Greek and Italian coasts, SWH >5 m were recorded (Varlas et al., 2023; Zimbo et al., 2022).

Based on the available data, Ianos was among the strongest Medicanes observed in the Mediterranean Sea in the last at least 25 years, both from a meteorological point of view (minimum pressure value, precipitation, strong wind gusts, and wave motion) and for the extensive damage to property, infrastructure, ports, agriculture. Furthermore, it caused four deaths (Lagouvardos et al., 2022). This Medicane reached category 2 on the Saffir-Simpson hurricane wind scale (Androulidakis et al., 2023).

2.8. Medicane "Apollo": 25 October-1 November 2021

On 25 October 2021, a low-pressure system formed near the Libyan coast. In the following days, during its northward motions, it became more intense, and on 28 October, it acquired the Medicane features. The effects of Apollo were observed, in particular, in Catania, Siracusa, and Ragusa provinces (Supplementary Fig. 1). Specifically, in the Catania province, a pluviometric mean of 200 mm/48 h (28–29 October) and a peak of 448 mm/48 h (near Linguaglossa, Supplementary Fig. 1) were recorded by the Sicilian Meteorological service ("Regione Siciliana – SIAS – Servizio Informativo Agrometeorologico Siciliano"), while on 29 October, >200 mm/24 h of rain and the highest wind gust (104 km/h) were recorded by SIAS in the Siracusa area. The minimum pressure value reached 999 hPa, and the sea wave activity also showed an intensification with SWH >3 m (Faranda et al., 2022).

After the Medicane transition, the Sicilian regional government declared a state of emergency for the 32 municipalities (in the provinces of Catania, Messina, Siracusa, and Ragusa) most severely affected by Apollo. The damage caused by Apollo was quantified at 2 million euros for what concerns the emergency interventions and at about 50 million for agriculture, productive activity, and infrastructure. Regarding the latter, damages were witnessed on the Catania-Siracusa highway due to the Simeto River overflowing, while the ports were affected by the intense wave motions, resulting in significant damage (Gazzetta Ufficiale Della Repubblica Italiana, n.d) last access 16/07/2023).

2.9. Common storms

In addition to the above-mentioned Medicanes, in this work, we also analyzed 4 "common" storms that occurred in the Ionian Sea and, similarly to most of the analyzed Medicanes, affected the eastern Sicily coast. These common storms took place during the following time intervals: i) 10–12 February 2015 (hereafter referred to as N1), ii) 20–23 December 2017 (N2), iii) 22–25 March 2021 (N3), and iv) 13–17 April 2021 (N4).

All these "common storms" were related to the occurrence of baroclinic instability, resulting from the combined action of air pressure and wind stress. These storms exhibited temporary sea-level rise caused by the inverse barometric effect and horizontal water column displacement due to wind stress, resulting in associated coastal flooding (Doodson, 1923; Lionello and Sanna, 2005; Lionello et al., 2006; Lionello, 2012). For the eastern part of Sicily, the main damage was not due to the rainfall but to the sustained wind gusts, which could reach a velocity of about 70 km/h and, consequently, to the storm surge induced by the wind.

For these storms, which had a limited space-time impact on the Eastern Sicily and Western Greek coastline in terms of damage, there was not much information. We obtained the SWH data from the hindcast maps provided by the Copernicus product MEDSEA_HINDCAST_WAV_006_012 (for additional information, see the Sea state data section) and the information about the wind gusts from the website "earth: a global map of wind, weather, and ocean conditions" (https://earth.nullschool.net/, last access 03/07/2023).

We focused on these 4 common storms since the storms N1 and N2 had already been analyzed, from a meteorological point of view, by Scicchitano et al. (2021), while the storms N3 and N4 represented 2 significant events recently occurred in the Mediterranean Sea.

All the considered common storms showed similar features in terms of SWH and wind gusts. The meteorological parameters, characteristic of the 4 common storms, are shown in Table 2.

3. Data and methods

For all the meteorological events taken into account, we choose the period to analyze in a way to involve the development of the event, the climax in terms of the minimum pressure value (only for the Medicanes), wind velocity, precipitation intensity, and SWH and the subsequent loss of power.

3.1. Seismic data

We used 104 seismic stations (Fig. 3a and Supplementary Table 1) installed along the Italian coastal areas, in the Sicily channel coastlines (in Malta, Lampedusa and Linosa islands), in Corsica Island and along the Greek and France coastal areas. Additionally, 15 seismic stations, installed in the Etnean area (Fig. 3b and Supplementary Table 2), were used to conduct array analysis. The selected seismic stations show specific characteristics: they are i) installed in coastal areas and ii) equipped with 3-component broadband seismic sensors. Seismic stations acquire with a sampling rate of 100 Hz. Noteworthy that the number of seismic

Table 2
Main meteorological features of the 4 analyzed common storms. All these meteorological parameters were derived from Hindcast Maps (SWH) and from the website "earth: a global map of wind, weather, and ocean conditions" (https://earth.nullschool.net/, last access 03/07/2023).

Name	N1	N2	N3	N4
Wind velocity (km/h)	50–65	60–70	50–55	40–55
SWH (m)	>3	>3	>3	>3
Duration (days)	3	4	4	3
Area with SWH > 3 m (km^2)	7.11E+05	6.27E+05	3.75E+05	1.69E+05
MRA (m^2/s)	0.6683	0.4624	0.2551	0.1849

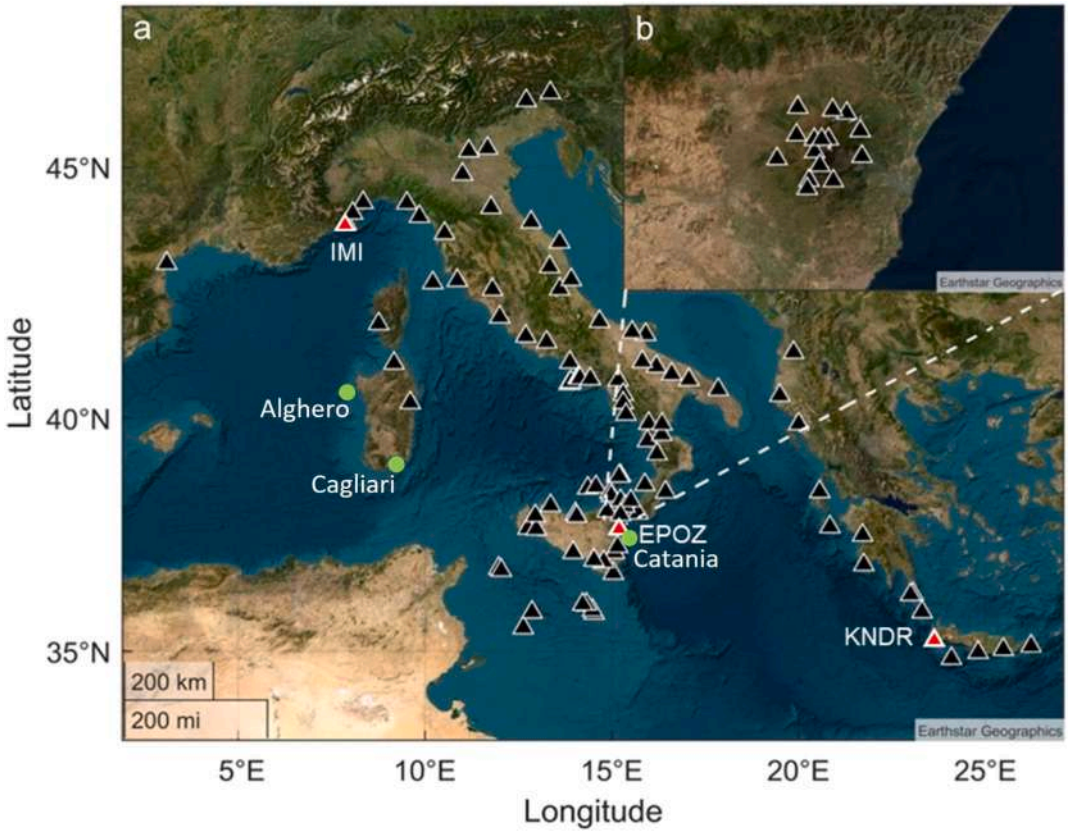

Fig. 3. Satellite image of the Mediterranean area with a selection of the broadband seismic stations available in the ORFEUS and INGV databases and used in the spectral analysis and the grid search method (a) and selection of the broadband seismic stations available in the Etna area maintained by INGV-OE (b), used in the array analysis. The red triangles indicate the stations used in the detailed analysis shown in Fig. 5 and Supplementary Figs. 3, 4, 5, 6 and 7. The green dots indicate the wave buoys used in this study. (base image source ©Earthstar Geographic).

stations available for each event could slightly vary as a consequence of station failure and of the date of installation. A detailed description of each station (name, latitude, longitude, altitude, sensor type and network) is presented in Supplementary Tables 1 and 2.

3.2. Sea state data

To obtain information about the sea state and the SWH, we used the "MEDSEA_HINDCAST_WAV_006_012" product, provided by the Copernicus Marine Environment Monitoring Service, and three wave buoys.

The Copernicus product contains the hindcast maps of the Mediterranean Sea Waves forecasting system and is based on the third-generation wave model WAM Cycle 4.5.4 (Zacharioudaki et al., 2019). In particular, the hourly SWH data was used to reconstruct the sea wave state during the periods taken into account (Fig. 3 and Supplementary Fig. 2).

Concerning the wave buoys, in Fig. 3a we show the locations of these buoys, located offshore of Alghero, Cagliari and Catania. These buoys are managed by ISPRA and are part of the Italian National Wave Buoy Network (RON) (Bencivenga et al., 2012). The instrumental equipment consists of buoys allowing the acquisition of wave parameters in real time. The long time series represent an important heritage for the knowledge of marine phenomena affecting the Italian seas, both in terms of climatology and extreme events. The RON National Wave Network is now composed of 7 stations located off the Italian coasts for the continuous measurement of wave and meteorological parameters, such as wind direction and speed, atmospheric pressure, water surface and air temperatures, with real-time data transmission. Data are collected continuously for periods of 20–25 min and are provided every 30 min.

The parameters recorded by the wave buoy and used in this study are: i) SWH (m), ii) wave mean period (s) and iii) wave mean direction (°).

We used Alghero, Catania and Cagliari buoys to obtain information about the sea state during Medicanes Rolf, Qendresa and Xandra, respectively (Fig. 2). We have no data on the other Medicanes since the RON ran until December 2014. The monitoring stations operating in the period 2009–2014 were Watchkeeper buoys from Axys, large particle-following buoys that use accelerometers, rate gyros and compasses to address the issues related to the small dimension buoys and to also guarantee a good platform for meteorological sensors. The particular tapered truncated cone hull shape and the accurate transfer function assure a good response in frequency and accuracy of wave height measurement. Semi-hourly sea state data, including SWH, periods and direction, are evaluated onboard, following several loaded procedures that return values in time and frequency domains, following Kahma et al. (2005) and Nondirectional and Directional Wave Data Analysis Procedure (2003). The new meteo-marine buoys, operating since 2021, were developed, designed and built in Italy for the specific needs of ISPRA, using the same philosophy of the described Watchkeeper buoys.

3.3. Spectral and amplitude analysis

The seismic data were corrected for the instrument response and thereafter spectral and amplitude analyses were performed. To perform the spectral analysis, the seismic signal was processed by Welch's method (Welch, 1967) using time windows of 81.92 s, leading to the calculation of hourly spectra. The hourly spectra, thus obtained, were gathered and represented as spectrograms, with time on the x-axis, frequency on the y-axis, and the $\log_{10}$ of the PSD indicated by a color scale. Examples of spectrograms obtained for the vertical component of

EPOZ, IMI and KNDR stations are shown in Fig. 5, for the Medicanes, and in Supplementary Fig. 3 for the common storms. Regarding the amplitude, we derived hourly time series of RMS amplitudes for the standard microseisms frequency bands: 0.2–0.4 Hz (SPSM, Supplementary Figs. 4 and 6), 0.1–0.2 Hz (SM, Fig. 5 and Supplementary Fig. 3), and 0.05–0.07 Hz (PM, Supplementary Figs. 5 and 7).

In addition, to show the spatial distribution of the RMS amplitude during the day when each Medicane and each common storm reaches its climax, we plotted the mean RMS amplitude computed on 1-day-long windows for the SM microseism band for the Medicanes (Fig. 6) and the common storm (Supplementary Fig. 8), for the PM (Supplementary Figs. 9 and 10) and SPSM (Supplementary Figs. 11 and 12). Each dot represents a seismic station and the color of the dot relates to the corresponding RMS amplitude at that location, as specified in the color bar. It is important to note that each color bar displayed represents a distinct range of RMS amplitude, effectively illustrating the varying response of the three analyzed microseism frequency bands (PM, SM, and SPSM) to the storm surge. This can be observed in Fig. 6 and Supplementary Figs. 8, 9, 10, 11 and 12.

3.4. Tracking Medicanes position

As the microseism is a continuous seismic signal, it is impossible to use the traditional techniques based on the first phase arrivals applied to localize the hypocenter of a seismic event. Therefore, we applied two different methods: i) grid search method, based on seismic amplitude-decay, and ii) array analysis.

3.4.1. Grid search method

We used the seismic signals recorded by 105 stations (Fig. 3a) to map out the position of the 8 Medicanes during their lifetime by employing a grid search approach (Fig. 7). This method, based on seismic amplitude decay, has already been used to track the source of the volcanic tremor at Mt. Etna (e.g., Di Grazia et al., 2006; Cannata et al., 2010) and recently to locate the source of microseism during the Medicane Apollo (Borzì et al., 2022). This method is based on an important assumption, specifically, we assume that the seismic waves are propagating inside a homogeneous medium (for further details about the method see Cannata et al., 2013). Furthermore, microseism amplitude was considered proportional to r^{-b}, where r is the source-station distance and the exponent b should be equal to 1 or 0.5 in the case of body or surface waves, respectively, in a way to take into account the geometrical spreading. The b exponent parameter was left unconstrained in the location procedure. To take into account also intrinsic attenuation, the frequency-dependent absorption coefficient α was considered in the range of 0–0.25 × 10^{-3} km^{-1} (Mitchell, 1995). Given that the microseism sources are located on the solid Earth's surface, the search was performed on a planar 2D grid roughly matching the Earth's surface. This is different from what is carried out on volcanoes where a 3D grid search is performed to take into account also deep seismic sources. The region, where we executed the grid search, is an area of 1610 × 2700 km (minimum longitude: −5°; maximum longitude: 30°; minimum latitude: 31.30°; maximum latitude: 45.90) with a spacing of 0.5° and we obtain one location every 4 h. As shown by Cannata et al. (2013) and by other authors implementing similar grid-search-based methods (for example Battaglia and Aki, 2003, who applied this method to localize rockfalls, long-period events, and eruption tremor sources on the Piton de la Fournaise volcano, or Kumagai et al., 2011, who localized the ascending seismic source during an explosive eruption at Tungurahua volcano), the selection of the grid spacing strikes a balance between achieving satisfactory spatial resolution and ensuring a reasonable computation time. The microseism source is localized based on the goodness of the linear regression fit (hereafter referred to as R^2) computed for each node of the bi-dimensional (2D) grid previously mentioned. Specifically, the source was positioned at the centroid of all grid nodes with R^2 values that deviated by no >1 % from the maximum R^2 value. To assess the reliability of the location findings, a statistical significance evaluation method was employed to analyze the retrieved maximum R^2 value. In particular, we performed 20 runs by randomly shuffling the RMS amplitude values among the stations. Then, we calculated the 99th percentile of the obtained values of R^2 and the results of this statistical method are shown in Table 3.

The grid search method used in this study shows various limits that in specific cases can invalidate the source locations. In particular, the first limit concerns the fact that in this method we consider the microseism source as a point-like source, while the microseism is produced in a wide area of the Mediterranean Sea. In this case, the point-like source is determined by locating the barycentric point of the extended source. However, it is important to consider the limitation posed by the presence of multiple sources that exhibit comparable intensity within the same frequency range. In such instances, the constrained source location adjusts toward a position between the actual seismic source locations (Battaglia et al., 2005), leading to a significant decrease in the R^2 value. In our case, we neglect localization that shows R^2 values smaller than R^2 indicated in Table 3 for each Medicanes, to avoid unreliable localization.

3.4.2. Array analysis

In order to track the location of all the Medicanes taken into account in this study, we also considered fifteen stations belonging to the Mt. Etna seismic permanent network and used them as a roughly circular array (Fig. 3b). The array analysis was performed to measure the apparent velocity and the back azimuth of the arriving wavefront of the microseism signal (e.g., Rost and Thomas, 2002). Most of the array techniques assume a planar propagation of the wavefront across the array based on the relationship between the sensor-source distances and the wavelength of the signal of interest (Havskov et al., 2016). The resolution of the array analysis depends on the geometry and size of the array, as well as on the wavelength of the seismic signal (Havskov et al., 2016). To consider a set of seismic stations as an array, three conditions have to be respected in their spatial configuration: (*i*) the aperture of the array should be greater than a quarter of the signal wavelength that we want to analyze (Aster and Scott, 1993); (*ii*) to avoid spatial aliasing, the wavelength of the signal should be at least comparable with the array interspacing (Asten and Henstridge, 1984); (*iii*) distances between array receivers and source of the signal must be greater than one wavelength (Havskov et al., 2016).

As shown by Borzì et al. (2022), the Array Response Function, performed for the three main microseism frequency bands, exhibits that the roughly circular array has a good response for the SM case.

In this study, we employed the f-k (frequency-wavenumber) analysis on the microseism signals, following the approach described by Rost and Thomas (2002). This method utilizes a beamforming technique in the spectral domain, conducting a grid search of slowness values to determine the back azimuth and apparent velocity that maximize the amplitude of the summed array traces. The outcome of the f-k analysis is a power spectral density as a function of slowness. Following the approach of Borzì et al. (2022), to apply array analysis to microseisms, we performed several processing steps on the seismic signals: (i) demeaning and detrending, (ii) bandpass filtering within the specific

Table 3
Significative R^2 values obtained by performing 20 runs by randomly shuffling the RMS amplitude values among the stations used in the grid search analysis.

Name	Data	Significative R^2
Rolf	6–9 November 2011	0.3251
Qendresa	7–8 November 2014	0.3141
Xandra	1–3 December 2014	/
Trixie	28 October - 1 November 2016	0.3863
Numa	15–19 November 2017	/
Zorbas	27–30 September 2018	0.2891
Ianos	15–20 September 2020	0.3270
Apollo	25 October - 1 November 2021	0.3298

microseism frequency band, (iii) segmenting into tapered windows of 60 s duration, (iv) excluding windows containing seismo-volcanic amplitude transients (e.g., volcano-tectonic earthquakes, long-period events, very long-period events) detected using the STA/LTA technique (Trnkoczy et al., 2012), and (v) applying the f-k analysis to each window by utilizing a slowness grid search (−1 to 1 s/km in the east and north components of the slowness vector) with a spacing of 0.05 s/km. Fig. 7 and Supplementary Fig. 13 illustrate examples of the obtained results.

3.5. Seismic signature of the Medicanes and common storms

To obtain the seismic signature and the main spectral characteristics of Medicanes and common storms, we use a method developed by Soubestre et al. (2018). This method was initially developed as a network-based method to detect and classify seismo-volcanic tremors. The proposed approach exploits the coherence of tremor signals across the network that is estimated from the array covariance matrix. Using this technique, as explained by Soubestre et al. (2018), it is possible to highlight both volcanic tremors and other types of seismic sources such as tectonic earthquakes (local, regional, and teleseismic), and oceanic seismic noise (microseism). This method allows to identify the spatially coherent individual noise source within the selected network, identified as small spectral width, as opposed to other noises such as local effects that would generate multiple individual sources. For further details about the method see Soubestre et al. (2018).

In this study, we use this technique both for the Medicanes and for the common storms to highlight the spectral content of these meteorological phenomena and to understand if the Medicanes and the common storm exhibit similar or different spectral characteristics. We perform this analysis only for the Medicanes that were localized by the grid search method since, only during these events more than one station clearly record an increment in the PSD and RMS amplitude. For this reason, this technique has not been applied to the Medicanes Xandra and Numa. Since we are interested in the microseism noise, we filtered the signal in the band 0.1–1 Hz and resample the signals at 25 Hz to speed up the computation time. To compute the covariance matrix, we use only the vertical component of the seismic signal and a window length of 60 s. The analyses were performed using the data recorded by a station set comprising stations installed both near the eastern Sicilian coast and the western Greek coast, in order to have the microseism source within the station set. We use this configuration for all the analyzed phenomena excluding the case of the Medicane Rolf, because, due to both the position of the Medicane and the spatial configuration of the 105 seismic stations used in our analysis, the only two seismic stations that "see" Rolf are installed in the Western part of the northern Italy. Also, the common storm N2 is an exception, as during this period (20–23 December 2017) the seismic stations installed near the Greek coastal area did not properly work and, for this reason, we use only three stations installed in the eastern part of Sicily.

3.6. Microseism reduced amplitude

Several authors tried to estimate the seismic intensity of tropical cyclones by using different methods. In particular, Gualtieri et al. (2018), in order to estimate tropical cyclones intensity from ambient seismic noise, work in two steps. Firstly, they derive a generalized linear model (GLM) of tropical cyclone intensity from the ambient seismic noise Power Spectral Density (PSD) using data between 2000 and 2010, and, secondly, use the estimation of the four GLM parameters to predict the intensity of Tropical cyclones during 2011 and 2012. In this work, they show that there exists a link between the intensity of the Tropical cyclones obtained from meteorological data and the increase of the PSD of the primary, secondary, and short-period secondary microseism.

To obtain the Microseism Reduced Amplitude (hereinafter MRA) of the 8 analyzed Medicanes and of the 4 common storms, we use this equation allowing to compute the MRA at each seismic station:

$$MRA = (d \text{ x } RMS) \quad (1)$$

where $\underline{d}$ is the source-station distance in meters (the source was derived from the previous localization analysis based on the seismic amplitude decay and we consider the Medicane a point-like source) and $\underline{RMS}$ is the value of the RMS amplitude, in m/s, recorded at the station in that specific time interval for the SM band. In particular, we calculate the magnitude of the Medicane only for the time interval when our localization analysis is considered reliable. Successively, to obtain a single value of seismic amplitude, characterizing a given Medicane, we test seven different sets of stations: i) the nearest 30 stations to the microseism source, ii) the nearest 40 stations to the microseism source, iii) the nearest 50 stations to the microseism source, iv) the stations located inside a circle with a radius of 300 km (the center of the circle is the microseism source), v) the stations located inside a circle with a radius of 400 km (the center of the circle is the microseism source), vi) the stations with RMS amplitude minor than the RMS amplitude of the station nearest to the source, and vii) finally all the 105 stations. The methods that consider a circle with a radius of 300 and 400 km were excluded because some Medicanes did not approach the coastline and the set contains only 3–4 stations. As the other sets of stations show very similar results in terms of magnitude, we choose the set that contains all 105 stations to have a station set for all the Medicanes as homogeneous as possible and we calculate the median between the 105 single values.

Using this equation, we multiply the RMS amplitude value recorded at the 105 seismic stations for the distance source-station in a way to take into account the attenuation due to the geometrical spreading. After obtaining a single value for each station we calculate the median value and, hence, we extract the seismic amplitude at the source characteristic of each Medicane.

In the case of the common storms, since they affect a larger portion of the Ionian Sea than the Medicanes and we are not able to localize it with the grid search method based on seismic amplitude decay, we consider as the source of the storm the centroid position of the area with SWH >3 m obtained from the hindcast maps (Supplementary Fig. 2). Thus, we are able to obtain the MRA also for the common storms and we can compare it with the Medicanes ones.

4. Results and discussion

In this work, we analyzed the relationship between the microseism and different meteorological events that occurred in the Mediterranean area between November 2011 and November 2021. In particular, we performed spectral and location analysis, and retrieved the seismic signature and the MRA both for Medicanes and common storms.

4.1. Spectral, amplitude and location analysis

In this section, we present and discuss the results of the spectral and location analysis performed for the Medicanes and the common storms taken into account. Borzì et al. (2022) showed that the microseism bands mostly showing the Medicanes effects are the SM and SPSM, and that the array analysis by using the Etna seismic stations is reliable only for the SM. Hence, we use the SM band to track the position of the 8 Medicanes analyzed in this work, while the spectral and amplitude analysis has been performed for the 3 microseism bands.

4.1.1. Rolf (6–9 November 2011)

The Medicane Rolf was the first Medicane monitored by the NOOA and one of the few Medicanes that developed in the Tyrrhenian Sea. The presence of this Medicane is clearly visible in the Ligurian seismic stations (such as IMI in Fig. 5). In particular, both the spectrograms and the RMS amplitude time series show an increase in the PSD and the RMS amplitude in the SM (Fig. 5) and SPSM (Supplementary Fig. 4) bands,

during the days 6–10 November 2011, highlighted by the vertical dashed line, in coincidence with the development, the climax, and the subsequent loss of power of the Medicane Rolf. As a result of the long distance Medicane - station, the other stations do not record any significant variations during this time interval. Also, the spatial RMS amplitude distribution, computed on 1-day-long windows, shows a cluster of high values in the Ligurian stations (Fig. 6a). We are able to locate the Medicane Rolf from 16:00 of 8 November to midnight of the day after (example in Fig. 7a).

4.1.2. Qendresa (7–8 November 2014)

Qendresa was a strong Medicane that, due to the high wind gust recorded in Catania (140 km/h) and in Malta (153 km/h), and the low minimum value pressure (985 hPa, Carrió et al., 2017; Bouin and Lebeaupin Brossier, 2020), led to the formation of sea waves with height >4 m (recorded by the Crotone and Catania wave buoys; Scicchitano et al., 2021). Qendresa is visible in all the stations installed in the Ionian area, highlighting the size of the area affected by the Medicane (Fig. 4b), while the stations installed in the Tyrrhenian area do not record significant variation during the lifespan of Qendresa. Also in this case, the Ionian stations (EPOZ and KNDR) show an increase in the PSD and in the RMS amplitude time series both for the SM (Fig. 5) and SPSM (Supplementary Fig. 4) bands. In addition, the RMS amplitude spatial distribution (Fig. 6b) shows very high values for south Italian and some Greek stations, confirming the large area affected by Qendresa.

Concerning the track of Qendresa, we are able to follow it during the

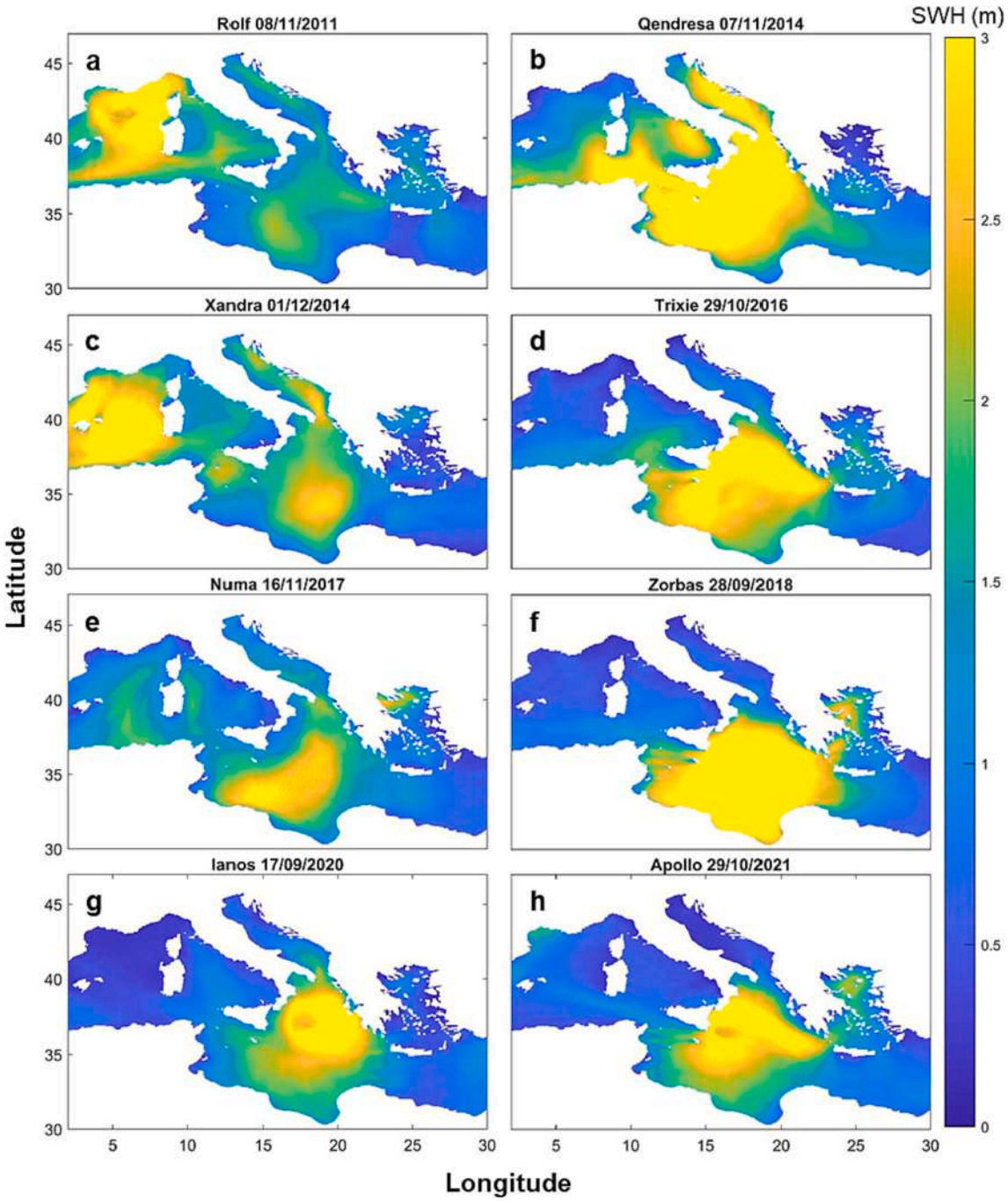

Fig. 4. Hindcast maps, obtained from the Copernicus product MEDSEA_HINDCAST_WAV_006_012, showing the spatial distribution of SWH during the day when each Medicane reaches its climax.

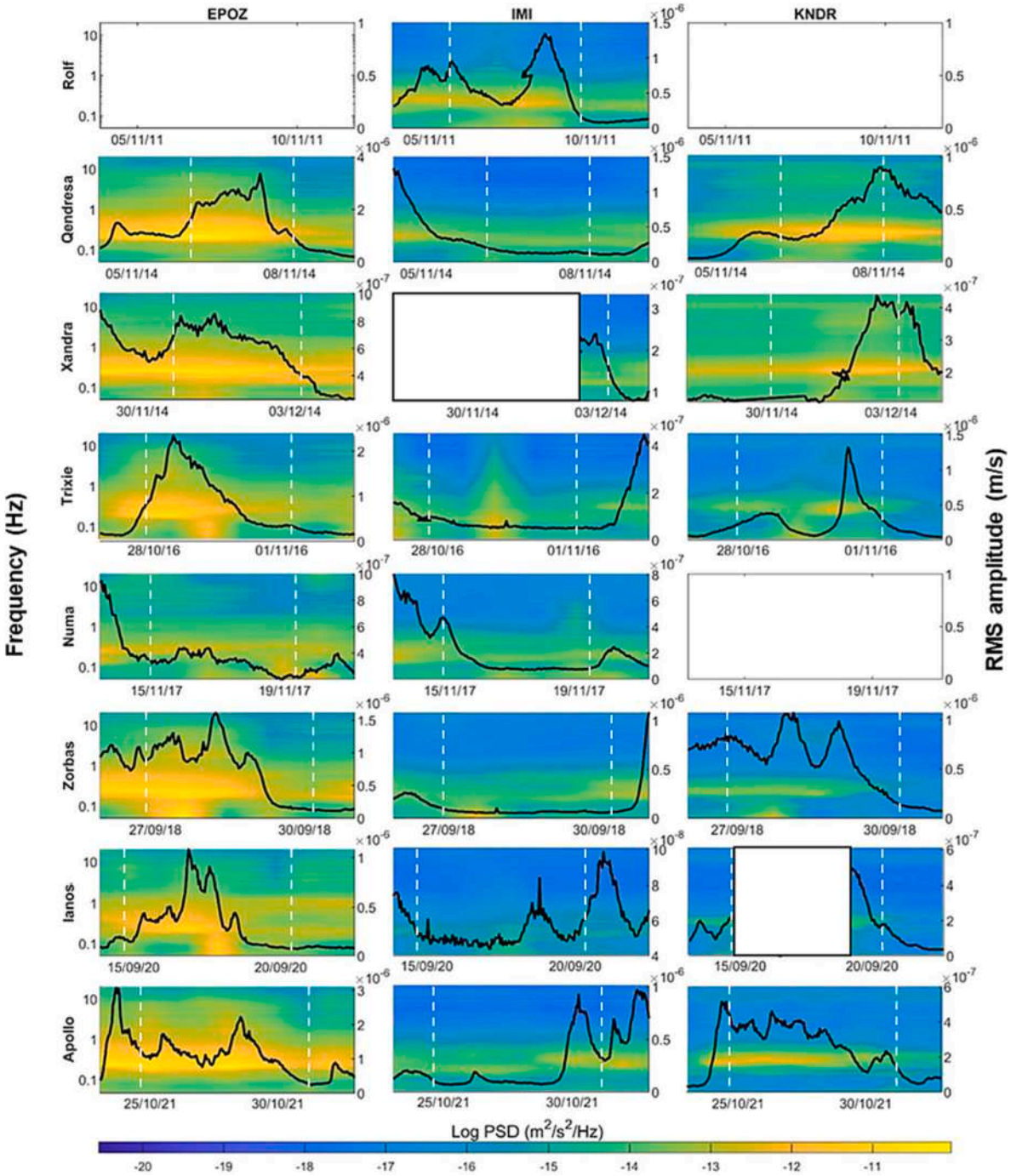

Fig. 5. Spectrograms and RMS amplitude time series for the SM band (0.1–0.2 Hz) of the seismic signal recorded by the vertical component of 3 stations located along the Sicilan (EPOZ), the Ligurian (IMI) and the Greek (KNDR) coastlines during the 8 Medicanes taken into account. The vertical dashed lines indicate the period taken into account in our analysis. See Fig. 3a for the station locations.

day 7 November from 4:00 to 16:00, which represents the time when the Medicane reaches its maximum intensity (example in Fig. 7b).

4.1.3. Xandra (1–3 December 2014)

Xandra is a small Medicane that occurred in the Tyrrhenian Sea during the days 1–3 December 2014. Despite the low minimum pressure value (989 hPa) and the diameter of about 200 km, it could not develop high wind speed (about 70 km/h; Di Muzio et al., 2019) and waves with significant heights >2 m. This is probably because its development was stopped by the first landfall that took place in Sardinia. After the Medicane reaches the Tyrrhenian Sea again but the small sea area available between the Sardinia and the Latium-Campania coast did not allow the full development of Xandra. The weak sea wave heights resulted in an insufficient energy transfer from the sea to the solid Earth. Only one station (AJAC) installed along the Sardinian coast shows a small amplitude increase in the SM band, while the other stations did not record any significant variation, as seen in spectrograms and RMS amplitude time series in Fig. 5. Also, the spatial RMS amplitude distribution computed for the day 1 December 2014 (Fig. 6c) does not show significant clusters of high values. For the same reason, we were unable to track the Medicane both by the grid search method and the array technique.

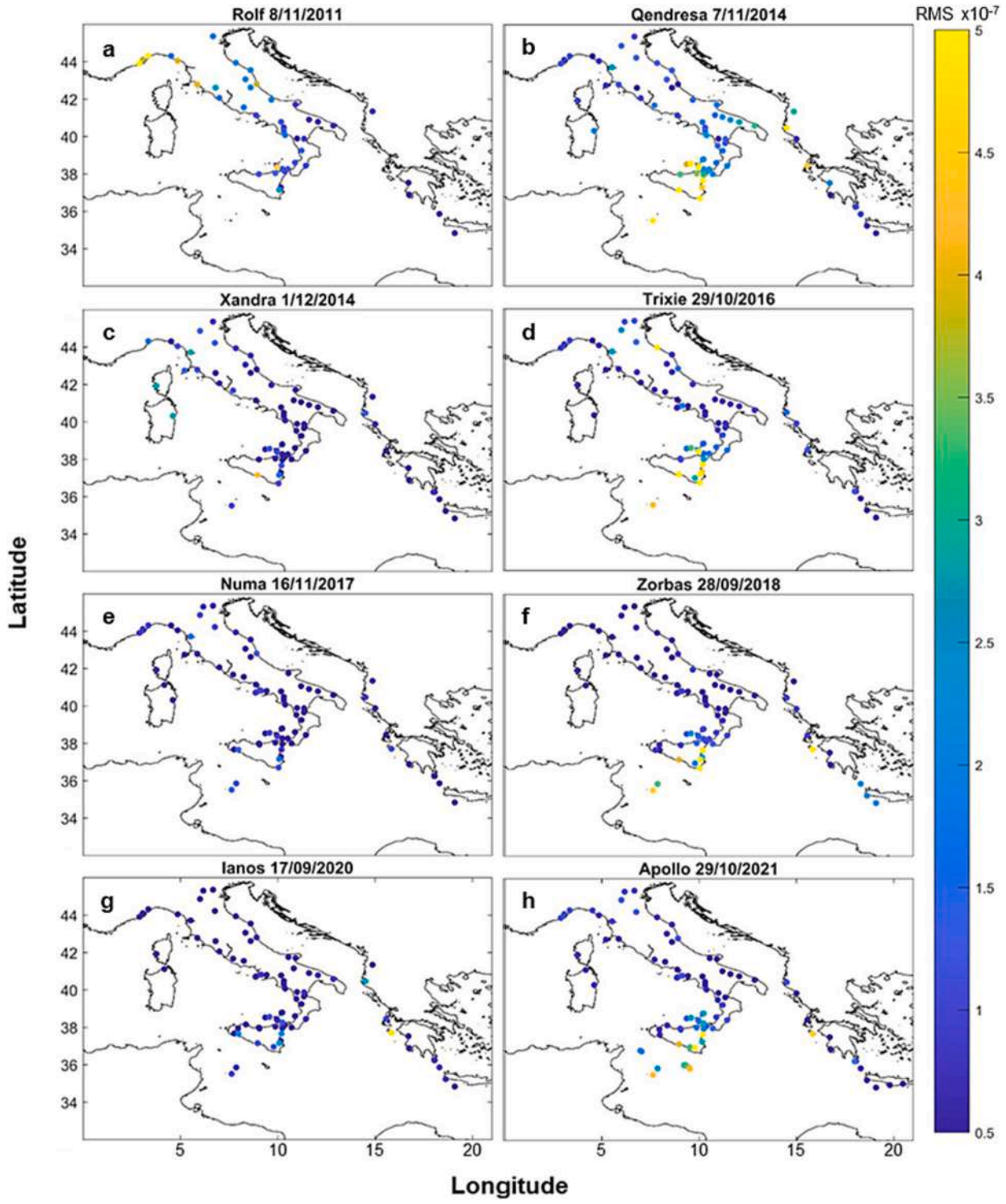

Fig. 6. Spatial distribution of the RMS amplitude for the SM band (0.1–0.2 Hz) computed at the 105 considered stations (dots) for the day when each Medicane reaches its climax. The colors of the dots represent the RMS amplitude as specified in the color bar.

The damage caused by the Medicane Xandra is associated with heavy rainfall and flooding, instead, there are no reports of damages caused by storm surges.

4.1.4. Trixie (28 October-1 November 2016)

Trixie was a Medicane that occurred in the Ionian Sea between 28 October - 1 November 2016. The minimum pressure value observed for this Medicane was one of the highest ever recorded (1002 hPa), and despite this during Trixie strong wind gusts, heavy rainfall and waves with significant waves heights >3 m were recorded (Di Muzio et al., 2019). In addition, the long lifetime of the Medicane has allowed an efficient energy transfer from sea waves to solid Earth, as explained in Ardhuin and Roland (2012) and Traer et al. (2012). All the Ionian stations show a distinct increase both in the PSD and in the RMS amplitude at the same time as the development of the Medicane (Fig. 5). Also, the RMS amplitude spatial distribution (Fig. 6c), computed for 29 October

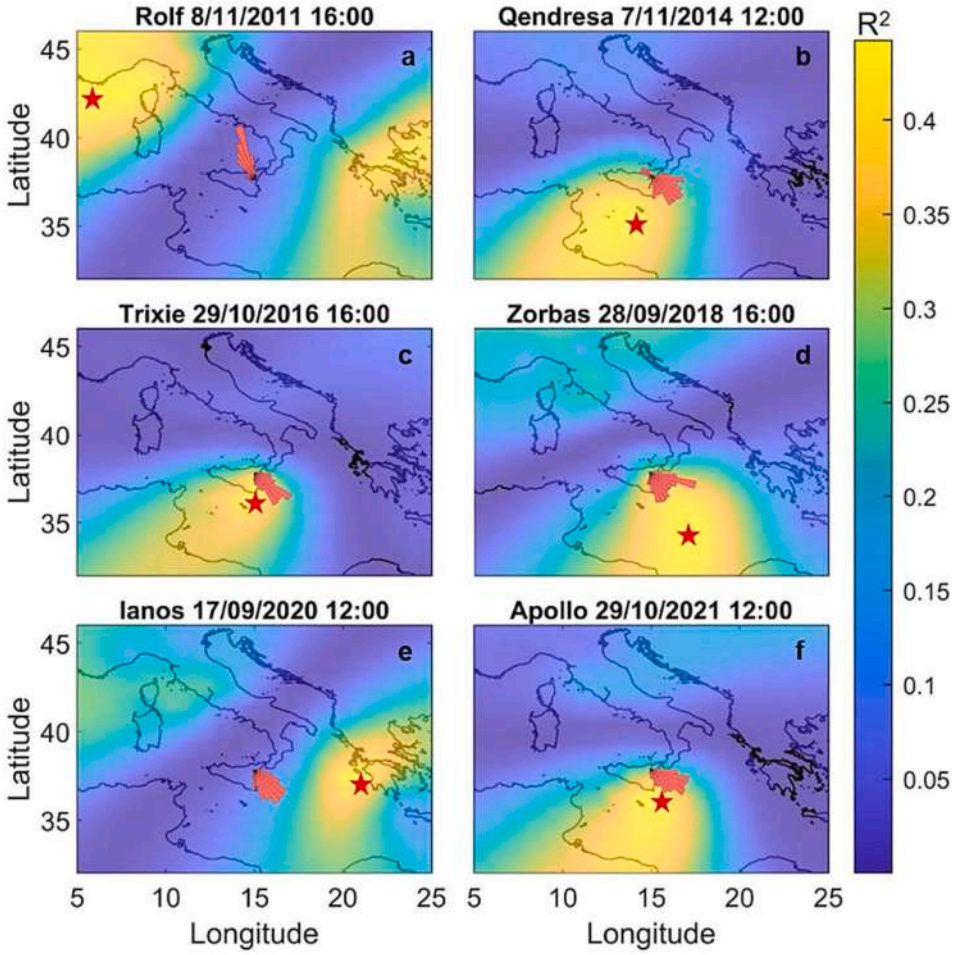

Fig. 7. Localization of the microseism source for the days when each medicanes reaches its climax. The red five-point star indicates the centroid position of all the grid nodes whose R^2 values do not differ by >1 % from the maximum R^2 value obtained with the grid search method, while the rose diagram, located at the center of the summit area of Mt. Etna (see Fig. 3b), shows the distribution of the back azimuth values on the same day obtained by array analysis.

when Trixie reached the maximum intensity, shows a cluster of very high values for the stations installed on the eastern Sicily coast, affected by waves with significant heights >3 m (Fig. 4d). As regards the tracking of this Medicane, we are able to follow its position for the entire day of 29 October 2016, obtaining six reliable locations (example in Fig. 7c).

4.1.5. Numa (15–19 November 2017)

Medicane Numa was a low-intensity Medicane that took place in the Ionian Sea during the time interval 15–19 November 2017. Although the size of the Medicane reaches a diameter of about 230 km, the minimum pressure value (1003 hPa) and the maximum recorded wind gust (72 km/h) testify to the low intensity of this Medicane (Rumora et al., 2018). In addition, the hindcast maps mostly show SWH smaller than 3 m (example in Fig. 4e). The Medicane is able to generate SWH higher than 3 m only for a few hours of the day 16 November 2017, when the Medicane was far from the Sicily coast. As explained in Ardhuin and Roland (2012) and Traer et al. (2012), a short-time interaction between intense wave motions (SWH > 3 m) and the sea floor is not able to efficiently convert the sea wave energy into microseism. In confirmation of this, as it is possible to observe in Fig. 6e, all the Ionian stations show low RMS amplitude values. For the same reason, also the localization analysis does not provide any reliable source locations for the Medicane Xandra.

4.1.6. Zorbas (27–30 September 2018)

Zorbas was considered one of the most energetic Medicane ever recorded on the Mediterranean Sea. From a meteorological point of view, two phenomena need to be highlighted: i) the waves reached SWH >5 m for a wide area of the Ionian Sea (Fig. 4f) and ii) the minimum pressure value reached a low value (990 hPa), while the wind speed and the rainfall showed rather low values (Varlas et al., 2020; Portmann et al., 2020; Scicchitano et al., 2020). All the Ionian stations, as shown in the spectrograms and RMS amplitude time series (Fig. 5) and spatial distribution (Fig. 6f), distinctly exhibit the presence of Zorbas. As regards the localization analysis, we can follow the Medicane from midday of 28 September 2018 to 8:00 of the next day (example in Fig. 7d).

4.1.7. Ianos (15–20 September 2020)

Ianos showed the lowest recorded values of minimum pressure (984 hPa) among the considered Medicanes and waves with heights >5 m (Lagouvardos et al., 2022; Zimbo et al., 2022). The presence of this Medicane is clearly visible in the spectrograms and in the RMS amplitude time series of all the Ionian stations (Fig. 5) and, in addition, one of the Greek stations used in our analysis (KNDR, Figs. 2 and 4 and Supplementary Figs. 4 and 5) stopped working due to the damages produced by the landfall of Ianos on the Greek coast. Also, the spatial distribution of the RMS amplitude shows a cluster of high values in all the Ionian stations (Fig. 6f). Ianos shows a first intensification during the first hours of 17 September, followed by a momentaneous loss of intensity and by a subsequent new intensification during the afternoon of the same day. Indeed, in our tracking analysis, we are able to follow the Medicane in the first hours of 17 September (from 00:00 to 04:00) and from 16:00 of the same day to 04:00 of the next day (example in Fig. 7e).

4.1.8. Apollo (25 October −1 November 2021)

Apollo was the last Medicane that occurred in late October 2021 in the Ionian Sea. Spectrograms, RMS amplitude time series (Fig. 5) and spatial distribution (Fig. 6h) clearly show the development, the climax, and the subsequent loss of power. As concerns the localization analysis, we are able to track Apollo for the entire day of 29 October 2021 (example in Fig. 7f).

4.1.9. Common storms

We also analyzed 4 common storms to understand if these storms present similar or different features compared with the Medicanes. All the addressed storms took place in the Ionian Sea and we can observe high PSD values and high RMS amplitude for all the seismic stations installed along the Ionian coastline for the SM (Supplementary Fig. 3) and SPSM bands (Supplementary Fig. 6), while no significant variation occurred for the PM band (Supplementary Fig. 7). Also, the RMS amplitude spatial distribution shows high values for the Ionian stations for the SM and SPSM bands (Supplementary Figs. 8 and 12, respectively). We try to locate these common seasonal storms by using the grid search method, but, while obtaining localizations in agreement with the real positions of the storms, the R^2 values turn out to be lower than the reliable R^2 threshold. Indeed, these storms simultaneously affect distant and large areas. For instance, the Sicilian, Calabrian, Apulian, Maltese, African and Greek coastline were affected by the N1 storm, hence every one of these areas can be considered as a source. We are therefore in the case of multiple sources that, as explained in the Data and methods section, invalidate our localizations. The array analysis, performed for the aforementioned 4 common storms, provides wavefront coming directions in agreement with the sea area that shows SWH >3 m (Supplementary Fig. 13).

4.2. The seismic signature of Medicanes and common storms

We use the covariance matrix method mainly to retrieve the seismic spectral content of the Medicanes and of the common storms, excluding local noise sources or local effects, and compare the results among them. In Figs. 8 and 9, we show the results of the covariance matrix (Fig. 8 a,b,c,d,e and Fig. 9 a,b,c,d,e), the maps with the tracks of the Medicanes (Fig. 8 a',b',c' and Fig. 9 a',b',c') and the area with SWH >3 m for the common storms (Fig. 8d',e' and Fig. 9d',e').

The main results of this analysis highlight that Medicanes and common storms show a different spectral content among them. In particular, Figs. 8 and 9, show that all the analyzed Medicanes (Apollo, Zorbas and Qendresa in Fig. 8a, b, c; and Ianos, Trixie and Rolf in Fig. 9a, b, c)display definite microseism spectral characteristics (between 0.18 and 0.35 Hz, corresponding to the SM and SPSM bands), while the common storms (Fig. 8d, e and Fig. 9d,e) exhibit a wider and higher spectral content (from 0.3 to 0.7 Hz).

As suggested in several works dealing with the relationship between microseism and different types of tropical cyclones (Gerstoft et al., 2006; Gualtieri et al., 2018; Lin et al., 2017; Retailleau and Gualtieri, 2019; Zhang et al., 2010), the distinctive spectral content of the Medicanes (0.18–0.35 Hz) highlights that all the types of cyclones, including the Medicanes, with their rotation and movement, are able to generate microseism in the SM and SPSM bands.

In the cases of the four common storms, the wider and higher spectral content could be related to the large area affected by the storm. Indeed, a huge difference between the common storms and the Medicanes lies in the extent of the sea area simultaneously affected by the wave height increase. Although the meteorological phenomena are stronger during a Medicane, the area affected by these extreme events is limited to 100–300 km, that is, on average, the diameter of a Medicane and, for this reason, a Medicane can be considered a point-like source. A common storm, even if with less intense phenomena, during its lifetime is able to involve the whole Mediterranean Sea. If we consider the particular case of an Atlantic perturbation, this initially affects the Tyrrhenian Sea and the western part of Italy, especially causing heavy rainfall, and, after, affects the Ionian Sea and the eastern part of Italy, causing strong wind gusts (50–70 km/h). Hence, the considered four common storms cannot be described as a point-like source, but these need to be considered as an extended source. Since the common storms affect a large area of the Mediterranean Sea and do not show a strong rotation around a minimum of pressure, like in the Medicane cases, the higher and wider spectral content, characteristic of these meteorological phenomena, needs to be investigated taking into account these two significant differences. The evidence abovementioned are able to explain the absence of high coherence values for frequencies smaller than 0.3 Hz highlighting that these phenomena are unable to generate SM while can produce SPSM as a consequence of local wave motions near the coastline.

The frequency higher than 0.3 Hz could be related to the interactions between waves with periods shorter than 6 s, presents in the Mediterranean Sea especially during the common storms (Agenzia per la Protezione dell'Ambiente e per i Servizi Tecnici, n.d), that generate pressure fluctuations propagating from the sea surface toward the sea bottom that, since the common storms affect a large area, show very different depths. This reason, together with the fact that the Ionian Sea is a relatively closed basin, could explain the higher and wider spectral content of the analyzed common storms. Indeed, during common storms, the vast area affected by waves with SWH > 3 m can generate resonance and reverb effects as a consequence of the coastal reflection (Guerin et al., 2022), resulting in the interaction between waves with various spectral characteristics. Indeed during a storm surge due to a common storm, the mean wave period recorded by the Italian wave buoy network shows a high percentage of waves with a period between 3 and 5 s followed by waves with a period between 5 and 7 s (Atlante delle onde nei mari Italiani - https://www.isprambiente.gov.it/it/pubblicazioni/rapporti/atlante-delle-onde-nei-mari-italiani. For extreme events like the Medicanes, we observe a longer wave period, varying from 8 to 10 s obtained from hindcast data. During the storms, the interaction between waves with shorter periods, due to the coastal reflection in a quasi-closed basin like the Ionian Sea, as highlighted in the PM, SM and SPSM definitions, leads to the generation of higher frequency microseism.

Some of the analyzed cases (Fig. 8b, d, e and Fig. 9b, d) show a change in the frequency during the time. In particular, Medicane Zorbas (Fig. 8b), Medicane Trixie (Fig. 8d), storm N1 (Fig. 8e) and partially N3 (Fig. 9d) show an increase in the frequency while the storm N4 (Fig. 8d) show a decrease in the frequency. This variation of the frequency can be explained by taking into account the sea depth. Indeed, as described in the literature (Gerstoft et al., 2006; Sun et al., 2013), the microseism frequency can be affected by the sea depth. In particular, Gerstoft et al. (2006) show that there is an increase in the frequency during the two landfalls of Hurricane Katrina and similar results are shown by Sun et al. (2013), who highlighted an increase in the intensity of the microseism for the SM and SPSM during the approaching of the three analyzed typhoons. Similarly, we obtained an increase of the frequency only for the Medicane that made landfall (Zorbas against Greek, Trixie against Cyprus) while for the other Medicanes (Apollo, Qendresa and Ianos), that did not approach the coast, we obtain a uniform trend without significant variations in frequency. The increase in the frequency of the common storms N1 and N3 could be explained considering that this type of perturbation, moving eastward, at first affects a deep-sea area (central part of the Ionian Sea, >2000 m deep) and successively a coastal area (Greek coastal area). The common storm N4 shows instead a unique trend with a decrease in frequency. If we focus on the area affected by this storm, we can observe that initially the storm affected an area characterized by shallow sea depth (Sicily channel with a maximum depth of 316 m), successively the storm moved to the Ionian Sea which is instead characterized by high depths (maximum depth of 5267 m). Hence, during this storm we see the opposite trend with respect to the Medicanes and the common storms N1 and N3.

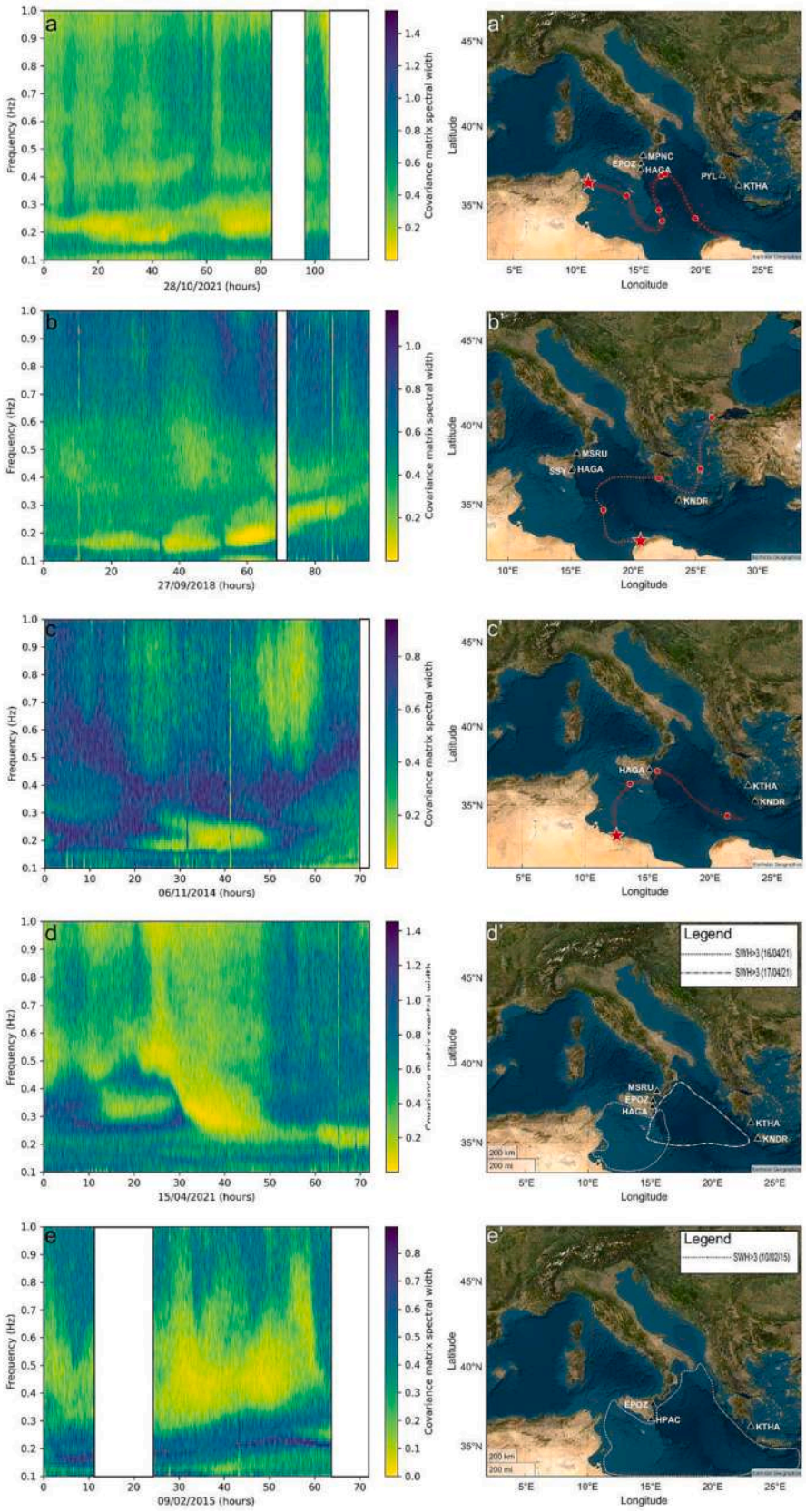

Fig. 8. Covariance matrix and maps with the station used to perform the analysis and the track of the Medicane Apollo (a and a'), Zorbas (b and b') and Qendresa (c and c'), and the area affected by SWH $>$ 3 for the storms N4 (d and d') and N1 (e and e'). The stars indicate the starting position of the Medicanes.

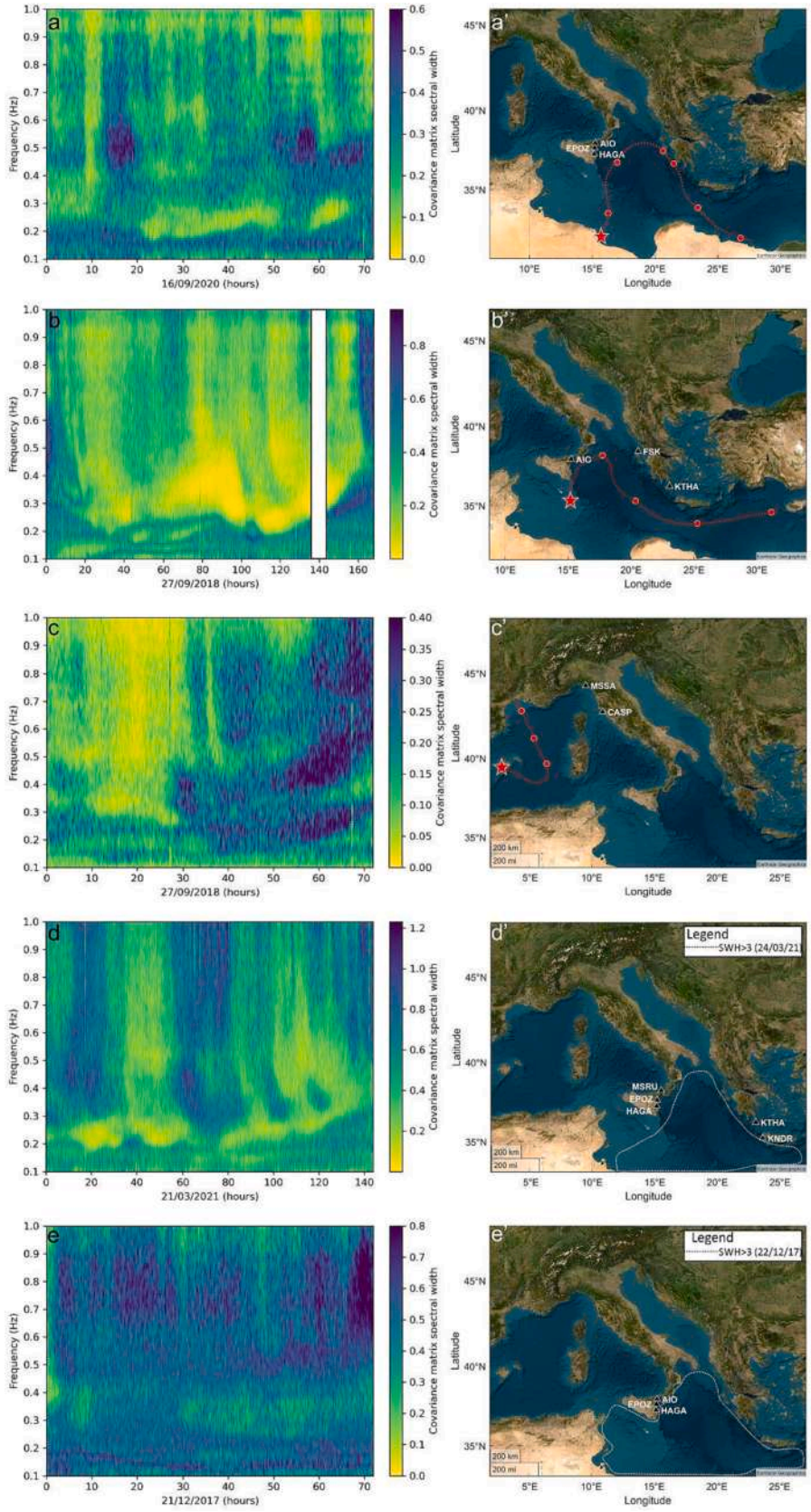

Fig. 9. Covariance matrix and maps with the station used to perform the analysis and the track of the Medicanes Ianos (a and a'), Trixie (b and b') and Rolf (c and c'), and the area affected by SWH > 3 for the storms N3 (d and d') and N2 (e and e'). The stars indicate the starting position of the Medicanes.

In the case of Medicanes, showing a very fast evolution like Qendresa (Fig. 8c), we can observe the focus of high coherence values in the SM and SPSM bands for a short time interval (about 30 h in this case), corresponding to the entire lifetime of the Medicane. A similar trend, even if not so clear, can be observed for the Medicanes Zorbas (Fig. 8b) and Ianos (Fig. 9a).

The common storm N3 (Fig. 8d) shows a seismic signature very similar to the Medicanes one, probably linked to the quasi-cyclonic shape.

4.3. The seismic strength of Medicanes and common storms

To calculate the strength of the Medicane and of the common storms from the seismic point of view, we use the reduced amplitude equation explained in the Data and methods section. From this analysis, two main findings were retrieved. The first concerns the fact that Medicanes and more common storms show significatively different values of MRA, while the second concerns the fact that for both the events this parameter is strongly correlated with the extent of the sea area with SWH >3 m.

Focusing on the Medicane case, we perform the analysis on 6 out of 8 events. Indeed, since to calculate the Microseism Reduced Amplitude it is necessary to locate the microseism source, we carry out this analysis only for the "localized" Medicanes. The results are summarized in Table 1. From these results, we can observe two sets of MRA values: the first comprises low values obtained for Trixie, Zorbas, Ianos and Apollo; the second higher values for Rolf and Qendresa. In addition, in Borzì et al. (2024), we analyze the relationship between the sub-tropical system Helios and microseism. Helios developed on the Sicily Channel during the period 9–11 February 2023. Based on satellite data, it is clear that this cyclone exhibits a warm core anomaly, a necessary condition for the formation of a Medicane. Nevertheless, this storm did not reach the status of a Medicane due to the absence of well-developed convection around the eye, which is a crucial requirement. In spite of this, Helios, due to its proximity to the Sicilian and Maltese coasts, was able to produce damage along these areas. In Borzì et al. (2024), we retrieve the microseism source, in agreement with the actual position of Helios, and the seismic signature of this event agrees with what we have obtained here for the cyclones. Hence, we extended the calculation of the MRA also for this Mediterranean cyclone.

Comparing the obtained MRA values with several meteorological parameters it is clear that the areal extent of the sea with significant wave heights >3 m influences the MRA, while the other meteorological parameters are not likely to be relevant for this analysis (Fig. 10). Indeed, observing Fig. 10 and Table 1, it is evident how an increase in the sea area extent with SWH >3 m corresponds with an increase in the MRA for all the Medicanes analyzed except for ROLF. We choose the SWH >3 m since this value represents the SWH threshold starting from which it is clear the correlation between the increase in the microseism energy (RMS and PSD) and the sea state. In particular, we observe the maximum MRA value, 0.1270 m^2/s, for the Medicane Qendresa, with a sea area affected by SWH >3 m of 6.25E+05 km^2 that is the largest area observed for the analyzed Medicanes, while the minimum value of MRA, 0.0359 m^2/s, is obtained for the Medicane Ianos showing the smallest area affected by SWH >3 m (1.34E+05 km^2). The MRA obtained for the Medicane ROLF is an outlier due to the unreliable computation of the MRA associated with this Medicane. Indeed, the position of Rolf is outside of the station network used in this work, and hence the distance between the South Italian, Greek and Maltese stations and the cyclone eye is very large. Presumably, the Ionian stations listen to local sources different from the Medicane source and hence by multiplying the RMS amplitude value recorded by the Ionian stations for the distance between these stations and the Medicane Rolf, we obtained MRA values unreasonably high. As mentioned before, the problem of multiple sources is also one of the main drawbacks of the grid search method based on seismic amplitude decay. To make things worse, Rolf occurred in 2011 and several stations used in our study had not yet been installed.

If we consider the MRA value obtained for the 4 common storms taken into account, we can observe that, as in the case of Medicanes, this parameter is strictly linked to the sea state and in particular to the extent of the area with SWH >3 m, thus highlighting that this areal parameter has a strong influence on the MRA (Table 2). Although MRA is clearly related to the extent of the area with SWH >3 m for both Medicanes and common storms, it is noteworthy that such a relationship is different in quantitative terms. Indeed, for the same extent of the area affected by high sea waves, the MRA computed for the common storms show higher values than the ones calculated for the Medicanes. If we consider the Medicane Qendresa and common storm N2, which show very similar areas affected by SWH >3 m, the value of MRA are 0.1270 m^2/s and of 0.4621 m^2/s, respectively. This evidence could suggest that during the common storms, the energy transfer between the sea waves and the solid Earth is higher and more efficient than during the Medicanes. During the Medicanes, and in general under cyclonic conditions, the generation of the SM is related to the rotary motion around the cyclone eye able to generate opposing waves with the same frequency (Lin et al., 2017). During common storms, the absence of a well-defined storm center, the

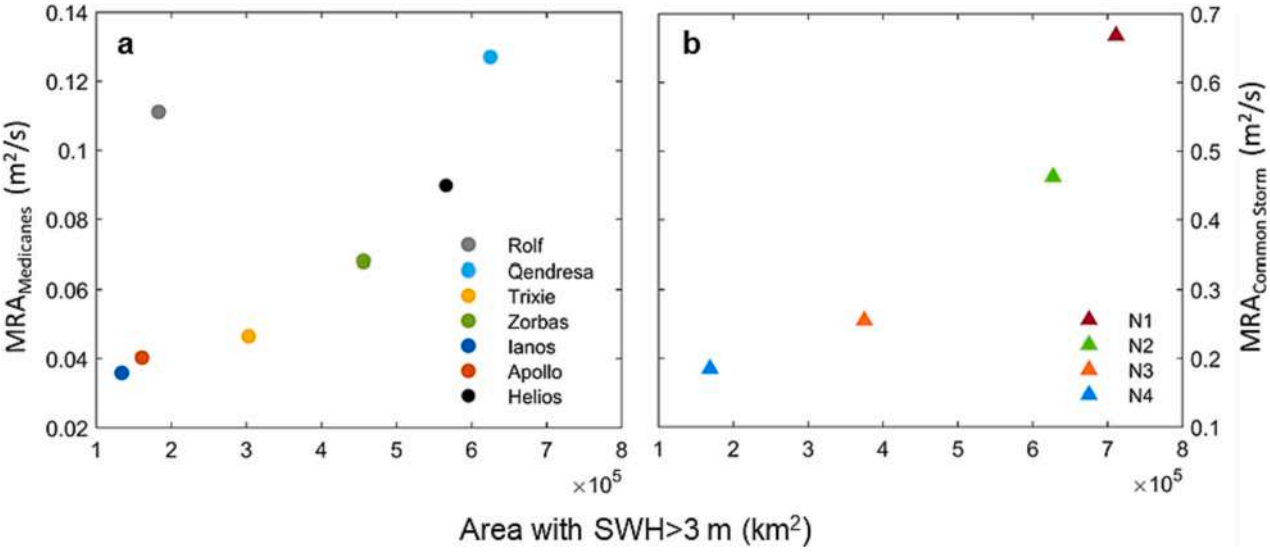

Fig. 10. scatter plot showing the MRA values in the y-axis and the area affected by SWH >3 m in the x-axis both for Medicanes (a) and common storms (b).

large extension of the sea area affected by the storm and the quasi-enclosed shape of the Mediterranean Sea could generate multiple and uncorrelated wave systems. As explained by Ardhuin et al. (2019), when the opposing waves are due to two uncorrelated wave systems, this typically gives a very strong noise and then a more intense microseism generation.

5. Conclusions

One of the primary goals in the modern seismology is to enhance our understanding of the interaction among the Atmosphere, Ocean, and Solid Earth (Lay et al., 2009). This study contributes to this objective by providing insights into meteorological events such as cyclones and common storms through the analysis of oceanic seismic noise. Over the past two decades, numerous studies have explored the connection between microseism and meteorological phenomena, with a focus on storm surges (Ardhuin et al., 2019; Cannata et al., 2020; Guerin et al., 2022; Moschella et al., 2020) and various kinds of cyclones (hurricanes, typhoons, tropical cyclones, and Medicanes; Borzì et al., 2022; Borzì et al., 2024; Bromirski, 2001; Bromirski et al., 2005; Gerstoft et al., 2006; Gualtieri et al., 2018; Lin et al., 2017; Retailleau and Gualtieri, 2019, 2021; Zhang et al., 2010).

In this study, we investigate the relationship between the three typical microseism bands (PM, SM, and SPSM) and several meteorological events that occurred in the Mediterranean Sea spanning from November 2011 to November 2021. Specifically, we examine eight Medicanes and four common storms that took place during this period.

To assess the sea state, hindcast maps for the entire Mediterranean Sea and data from three wave buoys (Alghero, Cagliari, and Catania) during Medicanes Rolf, Xandra, and Qendresa, respectively, are considered. Seismic analysis involves 120 stations along the Italian, Maltese, Greek, and French coastlines.

Spectral analysis results indicate that seismic signals, particularly in the SM and SPSM bands, are influenced by both Medicanes and common storms. The microseism amplitude in these bands increases during each Medicane and common storm, with a spatial RMS amplitude distribution in accordance with the event's location.

The main findings of this work concern two aspects: the assessment of the seismic signature of both Medicanes and common storms, and the calculation of the strength of these events from a seismic point of view. In particular, utilizing the covariance matrix method, we derive the seismic signatures for all the events taken into account, revealing significant differences between Medicanes and common storms. Medicanes exhibit typical microseism frequencies in the range of 0.18–0.35 Hz, aligning with the SM and SPSM bands that, as described in literature, are the microseism bands most affected by cyclonic activity. Common storms, in contrast, display a higher and wider frequency range (0.3–0.7 Hz). In addition, the Medicanes that conclude their life with a landfall show an increase in the frequency linked with the interaction with shallower seafloors in accordance with existing literature on hurricanes and typhoons.

Additionally, the MRA parameter provides information about the strength of both Medicanes and common storms from a seismic point of view. This parameter is closely linked to the sea state and in particular to the extent of the sea area with SWH >3 m. Common storms exhibit significantly higher MRA values than Medicanes, attributed to multiple and unrelated wave systems interacting in the quasi-enclosed Mediterranean Sea, hence common storms can transfer energy more efficiently.

This research, following Borzì et al. (2022) and Borzì et al. (2024), aims to study Mediterranean weather events by integrating microseism and sea state data. The main findings of this work pave the ways at the development of a multidisciplinary sea state monitoring system that integrates microseism data with the data recorded by the instruments routinely used for the sea state monitoring (such us wave buoys and HF Radar). In addition, the differences identified in both seismic signatures and MRA between Mediterranean cyclones and common storms allow us to seismically distinguish these two types of events. One of the future developments of this work could concern the application of the presented analyses to old digitized seismograms, to identify historical Mediterranean cyclones and analyze their temporal variability, in both occurrence rate and intensity, potentially linked to global warming (e.g., Emanuel, 2005; Reguero et al., 2019).

CRediT authorship contribution statement

Alfio Marco Borzì: Writing – review & editing, Writing – original draft, Methodology, Investigation, Formal analysis, Data curation. **Vittorio Minio:** Writing – original draft, Formal analysis. **Raphael De Plaen:** Validation, Methodology. **Thomas Lecocq:** Validation. **Flavio Cannavò:** Writing – original draft, Validation, Methodology, Conceptualization. **Giuseppe Ciraolo:** Validation, Formal analysis. **Sebastiano D'Amico:** Validation, Formal analysis. **Carlo Lo Re:** Validation, Formal analysis. **Carmelo Monaco:** Validation, Formal analysis, Data curation. **Marco Picone:** Writing – review & editing, Writing – original draft, Validation, Formal analysis, Data curation. **Giovanni Scardino:** Validation, Data curation. **Giovanni Scicchitano:** Validation, Data curation. **Andrea Cannata:** Writing – review & editing, Writing – original draft, Visualization, Validation, Supervision, Methodology, Conceptualization.

Declaration of competing interest

The authors declare that they have no known competing financial interests or personal relationships that could have appeared to influence the work reported in this paper.

Data availability

The seismic data, in the miniseed format used in this study, can be downloaded through the ORFEUS-EIDA database (http://www.orfeus-eu.org/data/eida/). All the seismic stations used in this study, along with their main features, are reported in Supplementary Tables 1 and 2. The hindcast data are available online on the Copernicus website (https://resources.marine.copernicus.eu/products).The wave buoys data are available online on www.mareografico.it and https://dati.isprambiente.it.

Acknowledgments

This research has been funded by the PRIN 2022 PNRR project titled "ARCHIMEDE - MultidisciplinARy approaCH to better define vulnerabIlity and hazard of MEDicanEs along the Ionian coasts of Sicily" (code P2022MJKMA, CUP H53D23011380001, E53D23021980001, B53D23033690001, Principal Investigator Prof. G. Scicchitano). The authors thank the i-waveNET "Implementation of an innovative system for monitoring the state of the sea in climate change scenarios" project, funded by the Interreg Italia-Malta Programme (https://iwavenet.eu/; notice 2/2019 Axis 3; project code C2-3.2-106). A.M.B. thanks the PON "Ricerca e Innovazione 2014-2020 Azione IV.5 - Dottorati su tematiche green". This study has been conducted using E.U. Copernicus Marine Service Information, doi:10.25423/cmcc/medsea_multiyear_wav_006_012. The seismic data, downloaded using the EIDA and ORFEUS webservices, belong to the AC (doi:https://doi.org/10.7914/SN/AC), FR (doi:10.15778/RESIF.FR), GU (doi:https://doi.org/10.7914/SN/GU), HC (doi:https://doi.org/10.7914/SN/HC), HL (doi:https://doi.org/10.7914/SN/HL), HP (doi:https://doi.org/10.7914/SN/HP), IV (doi:10.13127/SD/X0FXnH7QfY), ML (doi:https://doi.org/10.7914/SN/ML) and MN (doi:10.13127/SD/fBBBtDtd6q) networks. T.L. and R.D.P. thank the research project "SEISMOSTORM" funded by the BRAIN-be 2 program of the Federal Science Policy (BELSPO B2/202/P2/SEISMOSTORM). The authors thank three anonymous reviewers and the Associate Editor Christian Herrera for their

comments that helped improve our manuscript.

Appendix A. Supplementary data

Supplementary data to this article can be found online at https://doi.org/10.1016/j.scitotenv.2024.169989.

References

Agenzia per la Protezione dell''Ambiente e per i Servizi Tecnici. Dipartimento Tutela Acque Interne e Marine Servizio Mareografico - Atlante delle onde nei mari italiani - Università degli studi di Roma Tre. http://opac.apat.it/sebina/repository/catalogazione/immagini/pdf/atlante%20mari%201_60_2_.pdf.

Androulidakis, Y., Makris, C., Mallios, Z., Pytharoulis, I., Baltikas, V., Krestenitis, Y., 2022. Storm Surges during a Medicane in the Ionian Sea. Porto Heli, Greece, pp. 16–19.

Androulidakis, Y., Makris, C., Mallios, Z., Pytharoulis, I., Baltikas, V., Krestenitis, Y., 2023. Storm surges and coastal inundation during extreme events in the Mediterranean Sea: the IANOS Medicane. Nat. Hazards 117 (1), 939–978. https://doi.org/10.1007/s11069-023-05890-6.

Ardhuin, F., Roland, A., 2012. Coastal wave reflection, directional spread, and seismoacoustic noise sources. J. Geophys. Res. Oceans 117 (C11). https://doi.org/10.1029/2011JC007832.

Ardhuin, F., Gualtieri, L., Stutzmann, E., 2015. How ocean waves rock the earth: two mechanisms explain microseisms with periods 3 to 300 s. Geophys. Res. Lett. 42 (3), 765–772. https://doi.org/10.1002/2014GL062782.

Ardhuin, F., Stopa, J.E., Chapron, B., Collard, F., Husson, R., Jensen, R.E., Young, I., 2019. Observing sea states. Front. Mar. Sci. 124 https://doi.org/10.3389/fmars.2019.00124.

Asten, M.W., Henstridge, J.D., 1984. Array estimators and the use of microseisms for reconnaissance of sedimentary basins. Geophysics 49 (11), 1828–1837. https://doi.org/10.1190/1.1441596.

Aster, R.C., Scott, J., 1993. Comprehensive characterization of waveform similarity in microearthquake data sets. Bull. Seismol. Soc. Am. 83 (4), 1307–1314.

Battaglia, J., Aki, K., 2003. Location of seismic events and eruptive fissures on the Piton de la Fournaise volcano using seismic amplitudes. *Journal of Geophysical Research: Solid.* Earth 108 (B8). https://doi.org/10.1029/2002JB002193.

Battaglia, J., Ferrazzini, V., Staudacher, T., Aki, K., Cheminée, J.L., 2005. Pre-eruptive migration of earthquakes at the piton de la Fournaise volcano (Réunion Island). Geophys. J. Int. 161 (2), 549–558. https://doi.org/10.1111/j.1365-246X.2005.02606.x.

Bencivenga, M., Nardone, G., Ruggiero, F., Calore, D., 2012. The Italian data buoy network (RON). WIT Trans. Eng. Sci. 74, 321–332.

Borzì, A.M., Minio, V., Cannavò, F., Cavallaro, A., D'Amico, S., Gauci, A., Cannata, A., 2022. Monitoring extreme meteo-marine events in the Mediterranean area using the microseism (Medicane Apollo case study). Sci. Rep. 12 (1), 21363. https://doi.org/10.1038/s41598-022-25395-9.

Borzì, A.M., Minio, V., De Plaen, R., Lecocq, T., Alparone, S., Aronica, S., Cannata, A., 2024. Integration of microseism, wavemeter buoy, HF radar and hindcast data to analyze the Mediterranean cyclone Helios. Ocean Sci. 20 (1), 1–20. https://doi.org/10.5194/os-20-1-2024.

Bouin, M.N., Lebeaupin Brossier, C., 2020. Surface processes in the 7 November 2014 medicane from air–sea coupled high-resolution numerical modelling. Atmos. Chem. Phys. 20 (11), 6861–6881. https://doi.org/10.5194/acp-20-6861-2020.

Bromirski, P.D., 2001. Vibrations from the "perfect storm". Geochem. Geophys. Geosyst. 2 (7) https://doi.org/10.1029/2000GC000119.

Bromirski, P.D., Duennebier, F.K., Stephen, R.A., 2005. Mid-ocean microseisms. Geochem. Geophys. Geosyst. 6 (4) https://doi.org/10.1029/2004GC000768.

Cannata, A., Di Grazia, G., Montalto, P., Ferrari, F., Nunnari, G., Patanè, D., Privitera, E., 2010. New insights into banded tremor from the 2008–2009 Mount Etna eruption. *Journal of Geophysical Research: Solid.* Earth 115 (B12). https://doi.org/10.1029/2009JB007120.

Cannata, A., Di Grazia, G., Aliotta, M., Cassisi, C., Montalto, P., Patanè, D., 2013. Monitoring seismo-volcanic and infrasonic signals at volcanoes: Mt. Etna case study. Pure Appl. Geophys. 170, 1751–1771. https://doi.org/10.1007/s00024-012-0634-x.

Cannata, A., Cannavò, F., Moschella, S., Di Grazia, G., Nardone, G., Orasi, A., Gresta, S., 2020. Unravelling the relationship between microseisms and spatial distribution of sea wave height by statistical and machine learning approaches. Remote Sens. 12 (5), 761. https://doi.org/10.3390/rs12050761.

Carrió, D.S., Homar, V., Jansa, A., Romero, R., Picornell, M.A., 2017. Tropicalization process of the 7 November 2014 Mediterranean cyclone: numerical sensitivity study. Atmos. Res. 197, 300–312. https://doi.org/10.1016/j.atmosres.2017.07.018.

Cavicchia, L., von Storch, H., 2012. The simulation of medicanes in a high-resolution regional climate model. Clim. Dyn. 39, 2273–2290. https://doi.org/10.1007/s00382-011-1220-0.

Cavicchia, L., von Storch, H., Gualdi, S., 2014. Mediterranean tropical-like cyclones in present and future climate. J. Clim. 27 (19), 7493–7501. https://doi.org/10.1175/JCLI-D-14-00339.1.

Comellas Prat, A., Federico, S., Torcasio, R.C., D'Adderio, L.P., Dietrich, S., Panegrossi, G., 2021. Evaluation of the sensitivity of medicane ianos to model microphysics and initial conditions using satellite measurements. Remote Sens. 13 (24), 4984. https://doi.org/10.3390/rs13244984.

Dafis, S., Rysman, J.F., Claud, C., Flaounas, E., 2018. Remote sensing of deep convection within a tropical-like cyclone over the Mediterranean Sea. Atmos. Sci. Lett. 19 (6), e823 https://doi.org/10.1002/asl.823.

Di Grazia, G., Falsaperla, S., Langer, H., 2006. Volcanic tremor location during the 2004 Mount Etna lava effusion. Geophys. Res. Lett. 33 (4) https://doi.org/10.1029/2005GL025177.

Di Muzio, E., Riemer, M., Fink, A.H., Maier-Gerber, M., 2019. Assessing the predictability of Medicanes in ECMWF ensemble forecasts using an object-based approach. Q. J. R. Meteorol. Soc. 145 (720), 1202–1217. https://doi.org/10.1002/qj.3489.

Doodson, A.T., 1923. Meteorological perturbations of sea-level. Nature 112 (2821), 765–766. https://doi.org/10.1038/112765a0.

Emanuel, K., 2005. Increasing destructiveness of tropical cyclones over the past 30 years. Nature 436 (7051), 686–688. https://doi.org/10.1038/nature03906.

Faranda, D., Bourdin, S., Ginesta, M., Krouma, M., Noyelle, R., Pons, F., Messori, G., 2022. A climate-change attribution retrospective of some impactful weather extremes of 2021. Weather Clim. Dynam. 3 (4), 1311–1340. https://doi.org/10.5194/wcd-3-1311-2022.

Gazzetta Ufficiale Della Repubblica Italiana. https://www.gazzettaufficiale.it/eli/gu/2022/01/22/17/sg/pdf.

Gerstoft, P., Fehler, M.C., Sabra, K.G., 2006. When katrina hit California. Geophys. Res. Lett. 33 (17) https://doi.org/10.1029/2006GL027270.

Gualtieri, L., Camargo, S.J., Pascale, S., Pons, F.M., Ekström, G., 2018. The persistent signature of tropical cyclones in ambient seismic noise. Earth Planet. Sci. Lett. 484, 287–294. https://doi.org/10.1016/j.epsl.2017.12.026.

Guerin, G., Rivet, D., van den Ende, M.P., Stutzmann, E., Sladen, A., Ampuero, J.P., 2022. Quantifying microseismic noise generation from coastal reflection of gravity waves recorded by seafloor DAS. Geophys. J. Int. 231 (1), 394–407. https://doi.org/10.1093/gji/ggac200.

Hasselmann, K., 1963. A statistical analysis of the generation of microseisms. Rev. Geophys. 1 (2), 177–210. https://doi.org/10.1029/RG001i002p00177.

Haubrich, R.A., McCamy, K., 1969. Microseisms: coastal and pelagic sources. Rev. Geophys. 7 (3), 539–571. https://doi.org/10.1029/RG007i003p00539.

Havskov, J., Alguacil, G., Havskov, J., Alguacil, G., 2016. Seismic arrays. Instrumentation in earthquake seismology 309-329. https://doi.org/10.1007/978-3-319-21314-9_9.

Kahma, H., Krogstad, L., Monbaliu, W., 2005. Measuring and Analysing Directional Spectra of Ocean Waves. *COST Action 714*,. Bruxells.

Kerkmann J. and Bachmeier S. (2011). Development of a tropical storm in the Mediterranean Sea (6–9 November 2011). Available at: https://www.eumetsat.int/tropical-storm-develops-mediterranean-sea (last access: 07 February 2023).

Kumagai, H., Placios, P., Ruiz, M., Yepes, H., Kozono, T., 2011. Ascending seismic source during an explosive eruption at Tungurahua volcano, Ecuador. Geophys. Res. Lett. 38 (1) https://doi.org/10.1029/2010GL045944.

Lagouvardos, K., Karagiannidis, A., Dafis, S., Kalimeris, A., Kotroni, V., 2022. Ianos—a hurricane in the Mediterranean. Bull. Am. Meteorol. Soc. 103 (6), E1621–E1636. https://doi.org/10.1175/BAMS-D-20-0274.1.

Lay, T., Aster, R., Forsyth, D., Romanowicz, B., Allen, R.M., Cormier, V.F., Wysession, M. E., 2009. Seismological Grand Challenges in Understanding earth's Dynamic Systems. Report to the National Science Foundation, IRIS Consortium, p. 76.

Lecocq, T., Ardhuin, F., Collin, F., Camelbeeck, T., 2020. On the extraction of microseismic ground motion from analog seismograms for the validation of ocean-climate models. Seismol. Res. Lett. 91 (3), 1518–1530.

Lin, J., Lin, J., Xu, M., 2017. Microseisms generated by super typhoon Megi in the western Pacific Ocean. J. Geophys. Res. Oceans 122 (12), 9518–9529. https://doi.org/10.1002/2017JC013310.

Lionello, P. (Ed.), 2012. The Climate of the Mediterranean Region: From the Past to the Future. Elsevier.

Lionello, P., Sanna, A., 2005. Mediterranean wave climate variability and its links with NAO and Indian monsoon. Clim. Dyn. 25 (6), 611–623. https://doi.org/10.1007/s00382-005-0025-4.

Lionello, P., Malanotte-Rizzoli, P., Boscolo, R., Alpert, P., Artale, V., Li, L., Xoplaki, E., 2006. The Mediterranean climate: an overview of the main characteristics and issues. Develop. Earth Environ. Sci. 4, 1–26. https://doi.org/10.1016/S1571-9197(06)80003-0.

Longuet-Higgins, M.S., 1950. A theory of the origin of microseisms. Philos. Trans. R. Soc. Lond. A Math. Phys. Sci. 243 (857), 1–35. https://doi.org/10.1098/rsta.1950.0012.

Miglietta, M.M., Rotunno, R., 2019. Development mechanisms for Mediterranean tropical-like cyclones (medicanes). Q. J. R. Meteorol. Soc. 145 (721), 1444–1460. https://doi.org/10.1002/qj.3503.

Miglietta, M.M., Moscatello, A., Conte, D., Mannarini, G., Lacorata, G., Rotunno, R., 2011. Numerical analysis of a Mediterranean 'hurricane'over South-Eastern Italy: sensitivity experiments to sea surface temperature. Atmos. Res. 101 (1–2), 412–426. https://doi.org/10.1016/j.atmosres.2011.04.006.

Miglietta, M.M., Laviola, S., Malvaldi, A., Conte, D., Levizzani, V., Price, C., 2013. Analysis of tropical-like cyclones over the Mediterranean Sea through a combined modeling and satellite approach. Geophys. Res. Lett. 40 (10), 2400–2405. https://doi.org/10.1002/grl.50432.

Mitchell, B.J., 1995. Anelastic structure and evolution of the continental crust and upper mantle from seismic surface wave attenuation. Rev. Geophys. 33 (4), 441–462. https://doi.org/10.1029/95RG02074.

Moschella, S., Cannata, A., Cannavò, F., Di Grazia, G., Nardone, G., Orasi, A., Gresta, S., 2020. Insights into microseism sources by array and machine learning techniques: Ionian and Tyrrhenian Sea case of study. Front. Earth Sci. 8, 114. https://doi.org/10.3389/feart.2020.00114.

Nastos, P.T., Papadimou, K.K., Matsangouras, I.T., 2018. Mediterranean tropical-like cyclones: impacts and composite daily means and anomalies of synoptic patterns. Atmos. Res. 208, 156–166. https://doi.org/10.1016/j.atmosres.2017.10.023.

Nondirectional and Directional Wave Data Analysis Procedure, 2003. NDBC Technical Document 03–01. Silver Springs, MD: U.S. National Oceanic and Atmospheric Administration, National Weather Service, National Data Buoy Center.

NOOA. https://www.ssd.noaa.gov/PS/TROP/DATA/2011/tdata/med/01M.html.

Oliver, J., Page, R., 1963. Concurrent storms of long and ultralong period microseisms. Bull. Seismol. Soc. Am. 53 (1), 15–26. https://doi.org/10.1785/BSSA0530010015.

Portmann, R., González-Alemán, J.J., Sprenger, M., Wernli, H., 2020. How an uncertain short-wave perturbation on the North Atlantic wave guide affects the forecast of an intense Mediterranean cyclone (Medicane Zorbas). Weather Clim. Dynam. 1 (2), 597–615. https://doi.org/10.5194/wcd-1-597-2020.

Pravia-Sarabia, E., Gómez-Navarro, J.J., Jiménez-Guerrero, P., Montávez, J.P., 2021. Influence of sea salt aerosols on the development of Mediterranean tropical-like cyclones. Atmos. Chem. Phys. 21 (17), 13353–13368. https://doi.org/10.5194/acp-21-13353-2021.

Reguero, B.G., Losada, I.J., Méndez, F.J., 2019. A recent increase in global wave power as a consequence of oceanic warming. Nat. Commun. 10 (1), 205. https://doi.org/10.1038/s41467-018-08066-0.

Retailleau, L., Gualtieri, L., 2019. Toward high-resolution period-dependent seismic monitoring of tropical cyclones. Geophys. Res. Lett. 46 (3), 1329–1337. https://doi.org/10.1029/2018GL080785.

Retailleau, L., Gualtieri, L., 2021. Multi-phase seismic source imprint of tropical cyclones. Nat. Commun. 12 (1), 2064. https://doi.org/10.1038/s41467-021-22231-y.

Rost, S., Thomas, C., 2002. Array seismology: methods and applications. Rev. Geophys. 40 (3) https://doi.org/10.1029/2000RG000100, 2-1.

Rumora, I., Jukić, O., Filić, M., & Filjar, R. (2018). A study of GPS positioning error associated with tropospheric delay during Numa Mediterranean cyclone. Int. J. Trans. Traff. Eng., 8(3), 282-293.: https://doi.org/https://doi.org/10.7708/ijtte.2018.8(3).03.

Scardino, G., Scicchitano, G., Chirivì, M., Costa, P., Luparelli, A., Mastronuzzi, G., 2022. Convolutional neural network and optical flow for the assessment ofWave and tide parameters from video analysis (LEUCOTEA): an innovative tool for coastal monitoring. Remote Sens. 14, 2994. https://doi.org/10.3390/rs14132994.

Scicchitano, G., Scardino, G., Tarascio, S., Monaco, C., Barracane, G., Locuratolo, G., Mastronuzzi, G., 2020. The first video witness of coastal boulder displacements recorded during the impact of medicane "Zorbas" on southeastern Sicily. Water 12 (5), 1497. https://doi.org/10.3390/w12051497.

Scicchitano, G., Scardino, G., Monaco, C., Piscitelli, A., Milella, M., De Giosa, F., Mastronuzzi, G., 2021. Comparing impact effects of common storms and Medicanes along the coast of South-Eastern Sicily. Mar. Geol. 439, 106556 https://doi.org/10.1016/j.margeo.2021.106556.

Shaltout, M., Omstedt, A., 2014. Recent sea surface temperature trends and future scenarios for the Mediterranean Sea. Oceanologia 56 (3), 411–443. https://doi.org/10.5697/oc.56-3.411.

Soubestre, J., Shapiro, N.M., Seydoux, L., de Rosny, J., Droznin, D.V., Droznina, S.Y., Gordeev, E.I., 2018. Network-based detection and classification of seismovolcanic tremors: example from the Klyuchevskoy volcanic group in Kamchatka. J. Geophys. Res. Solid Earth 123 (1), 564–582. https://doi.org/10.1002/2017JB014726.

Sun, T., Xue, M., Le, K.P., Zhang, Y., Xu, H., 2013. Signatures of ocean storms on seismic records in South China Sea and East China Sea. Mar. Geophys. Res. 34, 431–448. https://doi.org/10.1007/s11001-013-9204-6.

Traer, J., Gerstoft, P., Bromirski, P.D., Shearer, P.M., 2012. Microseisms and hum from ocean surface gravity waves. *Journal of Geophysical Research: Solid.* Earth 117 (B11). https://doi.org/10.1029/2012JB009550.

Trnkoczy, A., Bormann, P., Hanka, W., Holcomb, L.G., Nigbor, R.L., Shinohara, M., Suyehiro, K., 2012. Site selection, preparation and installation of seismic stations. In *New Manual of Seismological Observatory Practice 2 (NMSOP-2)* (pp. 1–139). Deutsches GeoForschungsZentrum GFZ.

Varlas, G., Vervatis, V., Spyrou, C., Papadopoulou, E., Papadopoulos, A., Katsafados, P., 2020. Investigating the impact of atmosphere–wave–ocean interactions on a Mediterranean tropical-like cyclone. Ocean Model 153, 101675. https://doi.org/10.1016/j.ocemod.2020.101675.

Varlas, G., Pytharoulis, I., Steeneveld, G.J., Katsafados, P., Papadopoulos, A., 2023. Investigating the impact of sea surface temperature on the development of the Mediterranean tropical-like cyclone "Ianos" in 2020. Atmos. Res. 291, 106827 https://doi.org/10.1016/j.atmosres.2023.106827.

Welch, P., 1967. The use of fast Fourier transform for the estimation of power spectra: a method based on time averaging over short, modified periodograms. IEEE Trans. Audio Electroacoust. 15 (2), 70–73. https://doi.org/10.1109/TAU.1967.1161901.

Zacharioudaki, A., Ravdas, M., Korres, G., 2019. Mediterranean Production Centre MEDSEA_HINDCAST_WAV_006_012.

Zhang, J., Gerstoft, P., Bromirski, P.D., 2010. Pelagic and coastal sources of P-wave microseisms: generation under tropical cyclones. Geophys. Res. Lett. 37 (15) https://doi.org/10.1029/2010GL044288.

Zimbo, F., Ingemi, D., Guidi, G., 2022. The tropical-like cyclone "ianos" in September 2020. Meteorology 1 (1), 29–44. https://doi.org/10.3390/meteorology1010004.